arXiv:nucl-th/0409055v2 20 Sep 2005

Bulk effects in the coherent inelastic scattering of ultracold neutrons

A.L.Barabanov, S.T.Belyaev
Kurchatov Institute, 123182 Moscow, Russia

Abstract

With the use of theory developed earlier, bulk effects in ultracold neutron coherent inelastic scattering are considered both for solid and liquid target samples related to energy and momentum exchange with phonon and diffusion-like modes. For the neutron in a material trap, differential and integral probabilities for the energy transfer per bounce are presented in a simple analytic form which exhibits the parameter dependence. As an example, the theoretical values for the ultracold neutron loss rate from a storage bottle with Fomblin coated walls and stainless steel walls are evaluated. Possible contribution from incoherent inelastic scattering on hydrogen contamination is discussed.

PACS. 28.20.-v Neutron physics, 61.12.-q Neutron diffraction and scattering, 89.90.+n Other topics in areas of applied and interdisciplinary physics

1 Introduction

In the last few decades since the discovery [1, 2] of ultracold neutrons (UCN), great progress has been made in this field of physics. Now one considers UCN not only as a tool for studying fundamental properties of neutrons (life time and electric dipole moment) but also as a method for investigating material surfaces and thin films [3, 4].

The main specific feature of UCN is their repulsion from material samples, which allows storing them for a long time in material vessels. This repulsion results from rescattering of the neutron wave in the matter. Indeed, each atom in the target sample feels not only the incoming neutron wave but also the secondary waves from the other atoms. Effective secondary waves come mainly from surrounding volume $\sim \lambda^3$, where all $\sim n\lambda^3$ scatterers add coherently onto amplitude $\sim n\lambda^3(b/\lambda)$ (λ is the neutron wave length, b is the neutron-nucleus scattering amplitude, and n is the density of scatterers). This amplitude may be neglected, as compared to the incoming neutron wave, if $nb\lambda^2 \ll 1$. This is just the cases for thermal and cold neutrons but not true for ultracold neutrons. Thus, for the ultracold neutrons rescattering in the matter is of crucial importance, and for the wave vector $k < \sqrt{4\pi nb}$ (if $b > 0$) the rescattering becomes the dominant process and results in the total reflection from the surface. This dominant elastic scattering is simply described by a mirror potential $U = 2\pi\hbar^2 nb/m$, where m is the neutron mass.

Inelastic scattering of UCN on the trap walls also takes place and, in particular, (along with β-decay and radiative capture) results in UCN losses from the material vessels. For a long time attention was focused on the inelastic transition of UCN to the thermal energy region (upscattering), i.e. on large energy transfers (with probabilities per bounce 10^{-6} and higher). In the last few years the inelastic scattering with small energy transfers ("small heating" and "small cooling") was observed with probabilities per bounce 10^{-8}–10^{-6} (see, e.g. [5, 6, 7, 8, 9]). At the moment the data obtained for Fomblin oil as the sample appears to agree with theory. It was shown in [10], the small heating influences substantially the UCN losses from the traps with walls coated by Fomblin oil. The data on solids like stainless steel, beryllium and copper are controversial, in particular, no small heating was observed in [9] for non-magnetic solid substances (stainless steel, Be, Cu) with the upper bound of $\sim 10^{-8}$ for the probability per bounce.

Therefore, the inelastic UCN scattering is now of great interest, first due to the storage of UCN in material traps and, the second, for possible spectroscopic applications, e.g. for investigation of low frequency modes in surface layers and thin films [4]. On the other side, theoretical tools for the calculation of the inelastic scattering of UCN are rather undeveloped. One usually starts from Van Hove formula [11] for the differential cross section of neutron inelastic scattering on an ensemble of target nuclei,

$$\frac{d^2\sigma}{d\omega d\Omega} = \frac{k'}{2\pi k}\sum_{\nu,\nu'} b^*_\nu b_{\nu'} \int\limits_{-\infty}^{+\infty} dt\, e^{i\omega t}\langle i|e^{-i\mathbf{Q}\hat{\mathbf{R}}_\nu(t)}e^{i\mathbf{Q}\hat{\mathbf{R}}_{\nu'}(0)}|i\rangle. \tag{1}$$

Here and below we assume that $\mathbf{k}$ ($\varepsilon = \hbar^2k^2/2m$) and $\mathbf{k}'$ ($\varepsilon' = \hbar^2k'^2/2m$) are the wave vectors (energies) for incident and scattered neutrons, respectively, $\hbar\omega = \varepsilon - \varepsilon'$ and $\mathbf{Q} = \mathbf{k} - \mathbf{k}'$ are the neutron energy and momentum transfers, $\hat{\mathbf{R}}_\nu(t)$ is the time dependent Heisenberg operator of the ν-th nucleus position vector, and b_ν is the scattering amplitude on ν-th nucleus. The averaging is understood over the initial state $|i\rangle$ of the nuclear ensemble.

Note, however, that the Van Hove formula (1) is based on the Born approximation (see, e.g. [12, 13]) and, hence, does not imply rescattering. Strictly speaking, it may be applied only to thermal and cold neutrons (see also [14]).

Nevertheless, it is being used for UCN as the starting point for some tricky ansatz. First, one notes that the inelastic cross section, both for coherent and incoherent scattering, predicted by (1) is proportional to the total number of nuclei in the target. This allows to introduce the inelastic cross section for one nucleus. It should be stressed, that this definition is pure formal, because in fact the neutron is scattered by the whole sample as directly indicated by the presence of the correlation function in the right-hand side of (1). Then the resulting cross section for neutron-nucleus scattering may be somehow extrapolated from cold to ultra-cold energy region (say assuming $1/v$ law). The sum of this inelastic cross section and that for the radiative capture on one nucleus is considered as the cross section of the total loss, which is supposed to define the imaginary part of the neutron-matter optical potential (see e.g. [15, 16]). Some model modification of the Van Hove theory for UCN was attempted in [17].

Note, that the observed UCN losses are, as a rule, higher than that theoretically expected. With this respect one uses the term "UCN anomalous losses" (see, e.g. [18, 19, 20]). In fact, while one speaks of a discrepancy between experiment and theory, there is really a lack of a reliable theoretical description for UCN losses. We would like to emphasize, that the rescattering results in a drastic change in elastic neutron scattering when one goes from the cold to the ultra cold region. Thus, one can expect an important influence of this transition on the inelastic scattering. Thus, a theory of the inelastic scattering of UCN, based on solid grounds is, certainly, needed.

Recently, the authors presented a general theory of neutron scattering [14], valid for the whole domain of slow neutrons from thermal to ultracold. The target sample is considered as a dynamical system with the eigenstates $|j\rangle$ and the eigenvalues ε_j. The theory is in fact a method of the solution of the $N+1$ body Schroedinger equation for a "neutron + target nuclei" system. The only approximation, which was used, is based on the fact that the neutron-nucleus potential is short-range (as compared to an interatomic distance and a neutron wave length) and deep (as compared to neutron and target nuclei energies).

In this theory the amplitude of the neutron wave, ϕ, due to rescattering, is different at each nucleus, ν, of the sample and depends on the energy already transferred, i.e. on the target sample state, j. In other words, the quantity ϕ_ν^j is the neutron amplitude on the surface of the ν-th nucleus provided that the target sample is at the state j. These amplitudes are determined by a set of linear equations. The differential cross section takes the form:

$$\frac{d^2\sigma}{d\omega d\Omega}=\frac{k'}{2\pi k}\sum_{\nu,\nu'}\sum_{j,j'}\phi_\nu^{j*}\phi_{\nu'}^{j'}\times$$
$$\times\int\limits_{-\infty}^{+\infty}dt\,e^{i\omega t+i(\varepsilon_i-\varepsilon_j)t/\hbar}\langle j|e^{-i\mathbf{Q}\hat{\mathbf{R}}_\nu(t)}e^{i\mathbf{Q}\hat{\mathbf{R}}_{\nu'}(0)}|j'\rangle. \qquad (2)$$

It was shown that for thermal and cold neutrons, when rescattering is not important, the equations for ϕ_ν^j become very simple and result in $\phi_\nu^j\simeq\delta_{ij}b_\nu$. Thus, the cross section takes the Van Hove form (1). For the opposite case of ultracold neutrons, when rescattering becomes the dominant process, we have solved the equations for the amplitudes ϕ_ν^j. These amplitudes were presented as expansions in a small parameter $\mathbf{Qu}$, where $\mathbf{u}_\nu$ is the shift from the equilibrium position $\boldsymbol{\rho}_\nu$ of the ν-th nucleus in the target sample ($\mathbf{R}_\nu=\boldsymbol{\rho}_\nu+\mathbf{u}_\nu$).

The zero order in $\mathbf{Qu}$ corresponds to the scattering on the target sample with fixed, frozen (or infinitely heavy) nuclei and evidently can describe only elastic scattering. For inelastic scattering, one should consider the next orders in the small parameter $\mathbf{Qu}$. It is convenient to introduce the renormalized neutron amplitudes $\psi_j(\nu)\equiv e^{i\mathbf{k}\boldsymbol{\rho}_\nu}\phi_\nu^j/\beta_\nu$, and present them as series in $\mathbf{Qu}$

$$\psi_j(\nu)=\delta_{ij}\psi(\nu)+\psi_j^{(1)}(\nu)+\dots \qquad (3)$$

Here β_ν is the scattering length on the bound nucleus [14] (this quantity slightly differs from b_ν).

Zero order amplitudes $\psi(\nu)=\psi(\boldsymbol{\rho}_\nu)$ in the continuous media approximation were found to satisfy the Schroedinger equation with the optical potential $U(\boldsymbol{\rho})=2\pi\hbar^2n(\boldsymbol{\rho})\beta_c/m$, where β_c is the average ("coherent") scattering amplitude. Thus, the solution $\psi(\mathbf{k},\boldsymbol{\rho}_\nu)$ determines the zero order neutron amplitude on the surface of the ν-th nucleus inside a sample provided that the incident neutron has the wave vector $\mathbf{k}$.

Dynamical properties of the sample, and therefore the inelastic scattering, arise in the first order in $\mathbf{Qu}$. The corresponding cross section was obtained in the form

$$\frac{d^2\sigma_{ie}}{d\omega d\Omega}\sim\sum_{\nu,\nu'}\beta_\nu^*\beta_{\nu'}\nabla_\nu^i\left(\bar{\psi}(\mathbf{k}',\nu)\psi(\mathbf{k},\nu)\right)^*\times$$
$$\times\nabla_{\nu'}^j\left(\bar{\psi}(\mathbf{k}',\nu')\psi(\mathbf{k},\nu')\right)\int\limits_{-\infty}^{+\infty}\langle i|\hat{u}_\nu^i(t)\hat{u}_{\nu'}^j(0)|i\rangle e^{i\omega t}dt, \qquad (4)$$

where $\bar{\psi}(\mathbf{k},\nu)=\psi(-\mathbf{k},\nu)$ is to be interpreted as the wave function in the exit channel. Needless to say that the cross section (4) should be averaged over target initial states $|i\rangle$ with thermal equilibrium density matrix. Below such averaging is implied. We emphasize that the approximation $\mathbf{Qu}\ll 1$, which was used to derive Eq. (4), is valid for a wide range of neutron energies, from the ultra cold to the thermal region. Thus, all transitions within this range can be investigated on the same base.

In this paper we consider the case when the energies of initial neutrons are less than the barrier energy U. Therefore, the function $\psi(\mathbf{k},\boldsymbol{\rho})$ decreases rapidly inward from the surface of the target, namely at the lenght on the scale of 10 nm. Then, clearly, the notions like the total number of nuclei-scatterers and the inelastic cross section for one nucleus are senseless. We are not introducing them. In this sense, our approach is quite different from that commonly used for UCN [15, 16].

We are not introducing and discussing the imaginary part of the optical potential, caused by the inelastic scattering. In our approach [14], the functions of zero approximation, $\psi(\mathbf{k},\nu)$ and $\psi(\mathbf{k}',\nu)$, are determined by optical potential with the imaginary part, defined only by radiative capture. At the same time, Eq.(4) gives the cross section of inelastic neutron scattering on the whole target, even on macroscopic one.

Notice that in the paper [14] we have performed straightforward calculation of the total elastic cross section for a macroscopic plane sample and subbarier neutrons with the use of Eq.(2). It was shown that it coincides with the cross section of the sample seen by incoming neutrons (as it should be). Thus, the probability of inelastic scattering per one bounce by macroscopic sample can be calculated as the ratio of the inelastic and elastic cross sections. Just in this way the corresponding probability is calculated in our approach.

However, experiments with UCN in material traps do not allow a direct measurement of the differential cross section (4) or differential probability per bounce. Parameters which can be measured are the total loss rate (in particular, into the thermal region) and the energy distributions of pre- and post-storing neutrons. Since the probability of the small energy transfer is small, the multiple inelastic scattering of the same neutron may be neglected. Therefore, the energy spectrum of the stored neutrons can be directly linked to the total number of bounces with given material during the storage as well as to the probability of energy transfer per one bounce. In Section 2 we introduce the quantities measured in experiments, which will be analised and estimated.

The purpose of this paper is to demonstrate a real possibility to use our approach for analysis of the results of specific experiments on inelastic scattering of UCN. As the first step we assume that at the intrusion length of ~ 10 nm bulk properties of the matter are of dominant importance (discussion of the surface effects in the inelastic scattering, e.g. contribution from visco-elastic waves for Fomblin oil or from hydrogen thin films, see in [4, 10, 21, 22]). Thus, in a uniform material the diagonal matrix element $\langle i|\hat{u}^i_\nu(t)\hat{u}^j_{\nu'}(0)|i\rangle$ may exhibit a spatial dependence only as a function of $\boldsymbol{\rho}_\nu - \boldsymbol{\rho}_{\nu'}$ and therefore allows a Fourier transform

$$\langle i|\hat{u}^i_\nu(t)\hat{u}^j_{\nu'}(0)|i\rangle = \sum_{\mathbf{q},\omega} e^{i\mathbf{q}(\boldsymbol{\rho}_\nu - \boldsymbol{\rho}_{\nu'}) - i\omega t}\Omega^{ij}(\mathbf{q},\omega), \qquad (5)$$

where $\sum_{\mathbf{q}} = \int d^3q/(2\pi)^3$ and $\sum_\omega = \int d\omega/2\pi$. The correlation function $\Omega^{ij}(\mathbf{q},\omega)$ for the target material is the most uncertain factor in our approach. We analize it in Section 3.

Besides the usual phonon (sound) modes, we consider in details slow diffusion-like modes, namely, the contribution from thermo-diffusion and low frequency transverse modes in liquids. The idea is evident. Just the slow modes may be responsible for small energy transfer. However, for the sake of completeness, we perform calculation for all possible final neutron energies, from zero up to the thermal region. Earlier, the role of the thermo-diffusion in transition to the thermal region in solids was estimated in [17] and found insignificant.

Really, for crystals, the dominating contribution to the up-scattering (into the thermal region) is due to phonon processes with the momentum transfer to the lattice. Our result for this contribution coincides with that obtained early in a model approach, quite different from ours (see e.g. [18]).

All other processes, phonon- and thermo-diffusion ones, without lattice involvement, give small contribution into the scattering with large energy transfer. On the other hand, just these non-lattice processes are responsible for small energy transfers. In this paper, the corresponding probabilities for solids are calculated for the first time.

Moreover, in liquids and amorphous matter, non-lattice processes are the only ones responsible for the energy transfers, both small and large. Thus, in this paper, the contribution of bulk modes both to small and large energy transfers for liquids and amorphous samples are estimated also for the first time.

In the expression (4) we take into account all terms with $\nu \neq \nu'$ (as well as with $\nu = \nu'$), i.e. we calculate the coherent contribution to inelastic scattering. Thus, we use the average value (coherent scattering length) β_c instead β_ν in expressions for the inelastic cross section derived from (4). Note, that to evaluate the incoherent contribution related both to spin-flip and mixture of nuclei with different scattering lengths, one needs to separate additional term (proportional to β^2_{inc}) from the general equation (4) keeping only $\nu = \nu'$.

In this paper we restrict ourselves to the coherent inelastic scattering. Thus, we realize that our consideration is unsuitable for treatment of neutron scattering on targets with high hydrogen contamination. Our main goal is application to "hydrogen-free" materials.

As the starting point we use the following expression for the coherent inelastic cross section [14]:

$$\frac{d\sigma_{ie}}{d^3k'} = \frac{\hbar}{2\pi mk}\sum_{\mathbf{q}} B^{i*}(\mathbf{q})B^j(\mathbf{q})\Omega^{ij}(\mathbf{q},\omega), \qquad (6)$$

where

$$\mathbf{B}(\mathbf{q}) = \beta_c \sum_\nu e^{-i\mathbf{q}\boldsymbol{\rho}_\nu}\nabla_\nu\left(\bar{\psi}(\mathbf{k}',\nu)\psi(\mathbf{k},\nu)\right). \qquad (7)$$

It describes the transition of an incident neutron with the wave vector $\mathbf{k}$ into an element d^3k' of the final wave vector space $\mathbf{k}'$. This equation is valid for neutrons in a broad energy region, since the smallness of the parameter $\mathbf{Qu}$, that was used for deriving Eq.(6), is valid even for thermal neutrons. Indeed, for the latter, the scattering on the optical potential (~ 100 neV) is not important. Then, if one replaces the functions $\psi(\mathbf{k},\boldsymbol{\rho})$ and $\bar{\psi}(\mathbf{k}',\boldsymbol{\rho})$ by the plane waves $e^{i\mathbf{k}\boldsymbol{\rho}}$ and $e^{-i\bar{\mathbf{k}}'\boldsymbol{\rho}}$, respectively, then (6) transforms onto (1).

In this paper we consider the inelastic scattering of initial ultracold neutrons to any final energies, below and above the potential barrier. Of course, to calculate the neutron inelastic cross section from (6) and (7) one needs a specific model for the target sample to find solutions $\psi(\mathbf{k},\boldsymbol{\rho})$ and $\bar{\psi}(\mathbf{k}',\boldsymbol{\rho})$ for input and output channels. This problem is considered in Section 4.

In section 5 it is shown that multi-dimensional integration in (6) and (7) can be performed explicitly with realistic correlation functions. The details of the calculation are presented in Appendix. In section 6 we analyze how analytical results for differential probability are changed when specified for the excitation mode and energy transfer. In section 7 numerical results are presented for two typical substances, stainless steel and Fomblin oil. Results obtained, both analytical and numerical, are discussed in section 8. Conclusion is given in section 9.

2 UCN storage in material trap

2.1 Probability for energy transfer per one bounce

The probability for energy transfer per one bounce is naturally defined as a ratio of two cross sections, differential for energy transfer and the integral elastic one. The latter, in our case, is equal simply to the total sample area seen by the neutron, $S_\perp = Sk_\perp/k = S\cos\theta$, θ is the angle of incidence. With fixed initial wave vector $\mathbf{k}$ (or two its components $k_\perp$ and $k_\parallel$), the probability for the neutron after a bounce to have the kinetic energy ε' is

$$\frac{dw(k_\perp,k_\parallel\to\varepsilon')}{d\varepsilon'} = \frac{1}{S_\perp}\int \frac{d\sigma_{ie}}{d^3k'}\frac{d^3k'}{d\varepsilon'}. \tag{8}$$

In reality, the inelastic scattering of UCN with fixed $\mathbf{k}$ cannot be observed. One usually measures quantities somehow averaged over the initial momentum $\mathbf{k}$. Let us introduce a quasi-classical distribution $F(\mathbf{r},\mathbf{k})$ in position $\mathbf{r}$ and momentum $\mathbf{k}$ of UCN inside the trap, normalized by the condition

$$\int d^3r \int d^3k\, F(\mathbf{r},\mathbf{k}) = N_0, \tag{9}$$

where N_0 is the total number of UCN in the trap.

The number of neutrons, scattered by the element $d\mathbf{S}$ of the material sample at the position $\mathbf{r}_S$ (and height h_S) to the interval dE' of the total energy $E' = \varepsilon' + mgh_S$ during the time dt, is given by

$$dN = dE'dt \int d^3k\, F(\mathbf{r}_S,\mathbf{k})\ (\mathbf{v}\, d\mathbf{S})\ \times \\ \times\frac{dw(k_\perp,k_\parallel\to E'-mgh_S)}{dE'}, \tag{10}$$

where $\mathbf{v} = \hbar\mathbf{k}/m$ is the neutron velocity, and mgh_S is the neutron potential energy in the earth's gravitational field. The total rate of inelastic transition to the energy interval dE' is of the form

$$\frac{dN(E')}{dE'dt} = \oint dS \int\limits_{k_\perp>0} d^3k\, v_\perp F(\mathbf{r}_S,\mathbf{k})\times \\ \times\frac{dw(k_\perp,k_\parallel\to E'-mgh_S)}{dE'}. \tag{11}$$

Let us assume that the momentum distribution is isotropic, i.e. $F(\mathbf{r},\mathbf{k}) = F(\mathbf{r},k)$. Then, it is convenient to introduce a distribution $f(\mathbf{r},\varepsilon)$ in position and kinetic energy of UCN inside the trap

$$f(\mathbf{r},\varepsilon) = 2\pi\left(\frac{2m}{\hbar^2}\right)^{3/2}\sqrt{\varepsilon}\,F(\mathbf{r},k), \quad k=\sqrt{\frac{2m\varepsilon}{\hbar^2}}, \tag{12}$$

normalized by the condition

$$\int d^3r \int\limits_0^\infty d\varepsilon f(\mathbf{r},\varepsilon) = N_0. \tag{13}$$

Then, the transition rate takes the form

$$\frac{dN(E')}{dE'dt} = \oint dS \int\limits_0^\infty d\varepsilon\, v f(\mathbf{r}_S,\varepsilon)\frac{dw(\varepsilon\to E'-mgh_S)}{dE'}, \tag{14}$$

where

$$\frac{dw(\varepsilon\to\varepsilon')}{d\varepsilon'} = \langle\frac{dw(k_\perp,k_\parallel\to\varepsilon')}{d\varepsilon'}\rangle \tag{15}$$

is the differential probability of inelastic scattering averaged over the angle of incidence θ.

Here and below averaging of any function $f(k_\perp,k_\parallel)$ over θ is defined as

$$\langle f(k_\perp,k_\parallel)\rangle = \frac{1}{2}\int\limits_0^{\pi/2} d\theta\sin\theta\cos\theta\, f(k\cos\theta,k\sin\theta). \tag{16}$$

In the simplest approximation we neglect the earth's gravitational field, and assume, first, the density n_U of UCN in the trap is uniform over the volume and, second, the energy of UCN is fixed and equal ε_U, thus

$$f(\mathbf{r},\varepsilon) = n_U\delta(\varepsilon-\varepsilon_U). \tag{17}$$

The inelastic transition rate is of the form

$$\frac{dN(\varepsilon')}{d\varepsilon'dt} = Sn_Uv_U\frac{dw(\varepsilon_U\to\varepsilon')}{d\varepsilon'} \tag{18}$$

where S is the total area of the material surface inside the trap.

2.2 Probability for neutron losses from a trap

When the final neutron energy E' exceeds the barrier energy U, the neutron escapes from the trap. The probability of this event and the corresponding transition rate can be obtained as an integral over E' from U up to infinity from (14) (in the simplest approximation – as the similar integral over ε' from (18)).

The total escape probability is one of the quantities of practical interest. The second quantity of our interest is the small energy transfer. To be compared with measured values, both probabilities should be properly averaged over the energy and space distributions of the stored neutrons, and corrected for escape during the storage. Such averaging depends on the details of any specific experiment. On the other hand, the simple estimate (18) for the inelastic transition rate and its integral over ε' allow useful rough comparison with measured values.

3 Correlation function

In this section we consider the correlation function $\Omega^{ij}(\mathbf{q},\omega)$, entering Eq.(6). Correlation functions describe response (relaxation) of a substance after distortion of its statistical equilibrium by some external force characterized by ω and $\mathbf{q}$. Their structures for solids and liquids are covered in many books and articles on fluctuations and kinetics (see, e.g. [23, 24, 25, 26]). We restrict ourselves to the details necessary for what follows.

Fast distortions (when $|\omega| \gg \tau^{-1}$, where τ is some average relaxation time) are relaxed by phonons (or sound waves). In this region the correlation function can be easily obtained by expansion of the displacement vectors $\hat{\mathbf{u}}^i_\nu(t)$ in phonon amplitudes. The result is well known (see, e.g. Eq. (4.26) of Ref. [24]):

$$\Omega^{ij}(\mathbf{q},\omega) = \Omega^{ij}_l(\mathbf{q},\omega) + \Omega^{ij}_t(\mathbf{q},\omega), \tag{19}$$

where the longitudinal and transverse parts are given by

$$\Omega^{ij}_l(\mathbf{q},\omega) = \frac{q_i q_j}{q^2}\Omega_l(q,\omega), \tag{20}$$

$$\Omega^{ij}_t(\mathbf{q},\omega) = \left(\delta_{ij} - \frac{q_i q_j}{q^2}\right)\Omega_t(q,\omega), \tag{21}$$

and

$$\Omega_{l,t}(q,\omega) = \frac{2\hbar n_0(\omega)}{\rho c^2_{l,t}}\,\frac{\Gamma^2_{l,t}}{(q^2-\omega^2/c^2_{l,t})^2+\Gamma^4_{l,t}}. \tag{22}$$

Here $\rho = Mn$ is the material density (M is the nuclear mass), and

$$n_0(\omega) = \frac{1}{\exp(\hbar|\omega|/T)-1} \quad \underset{\hbar|\omega|\ll T}{\simeq} \quad \frac{T}{\hbar|\omega|} \tag{23}$$

is the occupation factor for a mode with the frequency ω at the temperature T. We allow the longitudinal (l) and transverse (t) sound velocities $c_{l,t}$ and damping factors $\Gamma_{l,t}$ to be different.

For isotropic solids, the factors $\Gamma^2_{l,t}$ can be taken proportional to the absorption coefficients of longitudinal and transverse sound (see, e.g. [27])

$$\Gamma^2_l = \frac{\gamma|\omega|^3}{c^4_l}, \quad \gamma = \frac{\zeta}{\rho} + \alpha D_S, \tag{24}$$

$$\Gamma^2_t = \frac{\nu|\omega|^3}{c^4_t}, \quad \nu = \frac{\eta}{\rho}. \tag{25}$$

Here η and $\zeta = 4\eta/3 + \varphi$ are the dynamic shear and longitudinal viscosities (φ is the volume viscosity), ν is the kinematic viscosity, $\alpha = C_P/C_V - 1$, where C_P and C_V are the specific heats for constant pressure and volume, respectively, $D_S = æ/\rho C_P$ is the thermo-diffusion coefficient (æ is the thermo-conductivity).

To describe a small energy exchange between UCN and a sample, the form of correlation function for small ω and q is of prime interest. Slow and long-range fluctuations are related to coherent motion of a great number of media atoms (hydrodynamic modes). For such kinds of distortion, local statistical equilibrium comes first and macro-relaxation by hydrodynamic processes follows. Therefore, in the region of small ω and q correlation functions for solids and liquids are governed by hydrodynamics and should depend on its parameters. Two different approaches, namely, phenomenological (from hydrodynamic fluctuations and Kubo theory [23, 24]) and quantum many-body theory [28], give the same result. In hydrodynamics two kind of processes (and corresponding correlations) are distinguished, longitudinal and transverse.

The longitudinal correlation function is related to "density–density" fluctuations

$$\frac{1}{2\pi N}\langle \int \hat{n}(\mathbf{r}'+\mathbf{r},t)\,\hat{n}(\mathbf{r}',0)\,d\mathbf{r}'\,\rangle = \sum_{\mathbf{q},\omega} e^{i\mathbf{q}\mathbf{r}-i\omega t} S(\mathbf{q},\omega), \tag{26}$$

where a Fourier transform, the "dynamical structure factor", can be shown to be connected with $\Omega_l(\mathbf{q},\omega)$ by

$$S(\mathbf{q},\omega) \simeq \frac{nq^2}{2\pi}\Omega_l(\mathbf{q}',\omega). \tag{27}$$

The vector $\mathbf{q}'$ in Ω_l is in the first Brillouin zone and $\mathbf{q}$, the momentum transfer, may differ from $\mathbf{q}'$ by a reciprocal lattice vector. In the right-hand side of (27), we omit all terms proportional to $\delta(\omega)$ and related to elastic scattering.

Following [23, 24] we get both for solids and liquids

$$\Omega_l(q,\omega) = \frac{T}{i\rho\omega}\left(\frac{1}{\omega^2 - c^2_{lT}q^2 - i\omega\Gamma_l(q,\omega)} - \text{c.c.}\right), \tag{28}$$

which looks like a phonon-type but with complicated form of "phonon absorption"

$$\Gamma_l(q,\omega) = \frac{(c^2_{lS}-c^2_{lT})q^2}{D_T q^2 + i\omega} + \frac{\zeta q^2}{\rho}, \tag{29}$$

where D_T is the thermo-diffusion coefficient. The subscripts T and S indicate constant temperature and entropy, respectively, and

$$\frac{c_{lS}^2}{c_{lT}^2} = \frac{D_T}{D_S} = \frac{C_P}{C_V} = 1 + \alpha. \tag{30}$$

For $q^2 \ll |\omega|/D_T$, Eqs. (28) and (29) result in the pure phonon-type correlation function with the sound velocity c_{lS} and the absorption defined by (24). For arbitrary small ω and q (hydrodynamic region)

$$|\omega| \ll \frac{c_l^2}{\gamma}, \quad q \ll \frac{c_l}{\gamma}, \tag{31}$$

the function (28) takes the form

$$\Omega_l(q,\omega) = \frac{iT}{\rho\omega} \times$$
$$\times \left(\frac{q^2 + i\omega/D_T}{c_{lT}^2 (q^2 + i\omega/D_S)(q^2 - \omega^2/c_{lS}^2 + i\omega^3\gamma/c_{lS}^4)} - \text{c.c.} \right). \tag{32}$$

It has two kind of poles, of phonon (p) and of thermo-diffusion (d) origin, and it is useful to separate them as

$$\Omega_l(q,\omega) = \Omega_l^p(q,\omega) + \Omega_l^d(q,\omega). \tag{33}$$

Here $\Omega_l^p(q,\omega)$ is given by (22) with Γ_l^2 (24) and

$$\Omega_l^d(q,\omega) = \frac{2T}{\rho c_{lS}^2 |\omega|} \frac{\alpha \Gamma_d^2}{q^4 + \Gamma_d^4}, \quad \Gamma_d^2 = \frac{|\omega|}{D_S}. \tag{34}$$

It is easy to see that additional diffusion-type pole in (32) originates from the pole in the "phonon absorption" $\Gamma_l(q,\omega)$ (29). The complicated structure of $\Gamma_l(q,\omega)$ is intrinsic only for longitudinal phonons.

The transverse correlation function for solids has only one, phonon-like, pole. So, transverse excitations in solids are relaxed only by phonons, and the correlation function for small ω and q has the same form (22) as for large q and ω.

In common liquid models, kinetics is assumed to go by finite jumps of atoms from one equilibrium position to the other after some average waiting time τ. For high frequencies $|\omega| \gg \tau^{-1}$ a liquid behaves like a solid. Low frequency waves ($|\omega| \ll \tau^{-1}$) damp due to viscosity. This limit is reproduced by the correlation function for the liquid model with one relaxation time (see, e.g. [23])

$$\Omega_t(q,\omega) = \frac{T}{i\rho c_t^2 q^2} \left(\frac{1}{\omega - i\Gamma_t(q,\omega)} - \text{c.c.} \right), \tag{35}$$

where

$$\Gamma_t(q,\omega) = \frac{c_t^2 q^2 \tau}{1 + i\omega\tau}. \tag{36}$$

The relaxation time is usually estimated as $\tau = \eta/G = \nu/c_t^2$, where η and $\nu = \eta/\rho$ are dynamic and kinematic shear viscosities, respectively, G is the modulus of elasticity, and $c_t^2 = G/\rho$.

The correlation function (35) and (36) exactly transforms to the form (22) with the damping factor

$$\Gamma_t^2 = \frac{|\omega|}{c_t^2 \tau} = \frac{|\omega|}{\nu}. \tag{37}$$

Note, that for low frequencies

$$|\omega| \ll \tau^{-1} = \frac{c_t^2}{\nu} \tag{38}$$

there exists a wide hydrodynamic region for q

$$\frac{|\omega|}{c_t} \ll q \ll \frac{c_t}{\nu}, \tag{39}$$

where the Eq.(35) (as well as (22)) transforms into the diffusion-type function (34) with damping factor (37). It is of interest that this factor is proportional to ν^{-1} in contrast to (25) (see, e.g. [29]).

The correlation functions can be determined from first principles only for two limiting areas of variables, large and small ω and $\mathbf{q}$. In the intermediate area one should use some specific interpolation models for the substance considered.

Thus, we use the correlation function as a sum of phonon- and diffusion-type terms. Contribution to the cross-section from each part can be calculated independently and summed afterwards.

For the calculation of the cross-section we will need $\Omega(\mathbf{q},\omega)$ as a function of $q_\perp$ ($q^2 = q_\perp^2 + q_\parallel^2$), and it is convenient to present all cases considered above in the same form

$$\Omega(q_\perp) = \frac{2\alpha\hbar n_0(\omega)}{\rho c^2} \bar{\Omega}(q_\perp), \tag{40}$$

where

$$\bar{\Omega}(q_\perp) = \frac{\Gamma^2}{(q_\perp^2 + p^2)^2 + \Gamma^4}, \quad p^2 = q_\parallel^2 - \frac{\epsilon\,\omega^2}{c^2}, \tag{41}$$

and $\alpha = \epsilon = 1$ for all cases besides the longitudinal thermo-diffusion mode. In the latter case we have $\alpha = C_P/C_V - 1$ and $\epsilon = 0$.

Note, that Γ_p^2 (phonon absorption) is a small parameter for all values of ω and q that we are considering, and when $\Gamma_p \to 0$,

$$\bar{\Omega}_p(q_\perp) \quad \longrightarrow \quad \pi\delta\left(q^2 - \frac{\omega^2}{c^2}\right), \tag{42}$$

in agreement with the phonon correlation function usually used.

4 Specific target sample: uniform thick layer

In this section we will derive the function $\mathbf{B}(\mathbf{q})$ (7) for a simple model commonly relevant to the UCN storage experiments, i.e. an uniform thick layer. The appropriate choice of the model allows us to define the solutions $\psi(\mathbf{k},\boldsymbol{\rho})$ and $\bar{\psi}(\mathbf{k}',\boldsymbol{\rho})$ of the Schroedinger equation with optical potential for input and output channels.

The problem is that the function $\psi(\mathbf{k},\nu)$, being the neutron amplitude at the ν-th nucleus, is defined only inside the sample. But to get $\psi(\mathbf{k},\nu)$ in the continuous media approximation, one has to find the scattering type solution of the Schroedinger equation with an external plane wave entering the sample, $e^{i\mathbf{k}\boldsymbol{\rho}}$. For the input channel function, $\psi(\mathbf{k},\nu)$, one may imagine the external plane wave as attributed to the incoming neutron. Let us assume it to come from the left. For the output channel function, $\bar{\psi}(\mathbf{k}',\boldsymbol{\rho}) = \psi(-\mathbf{k}',\boldsymbol{\rho})$, the corresponding external wave, $e^{-i\mathbf{k}'\boldsymbol{\rho}}$, is an auxiliary quantity and should be directed to the right, for back scattering, and to the left, for forward scattering.

To include both cases, let us consider a uniform layer located at $-a/2 < z < a/2$ with the surface area S and the thickness a, much larger than the incident neutron wave length. The sample is supposed to have the density n and the scattering length β_c providing a constant optical potential U. Note that in a general case, β_c is complex with an imaginary part that can be used to describe the radiative capture of UCN.

We consider two solutions of the model scattering problem, described above, with the left (L) and right (R) incoming waves. Outside the target they have the form

$$\psi^{(L)}(\mathbf{k},\mathbf{r}) = e^{i\mathbf{k}_\parallel\mathbf{r}_\parallel}\cdot\begin{cases} e^{ik_\perp z} + R\,e^{-ik_\perp z}, & z < -a/2,\\ T\,e^{ik_\perp z}, & z > a/2,\end{cases} \tag{43}$$

$$\psi^{(R)}(\mathbf{k},\mathbf{r}) = e^{i\mathbf{k}_\parallel\mathbf{r}_\parallel}\cdot\begin{cases} T\,e^{-ik_\perp z}, & z < -a/2,\\ e^{-ik_\perp z} + R\,e^{ik_\perp z}, & z > a/2.\end{cases} \tag{44}$$

In both cases $k_\perp \equiv |\mathbf{k}_\perp| > 0$ is the normal component of the neutron momentum, and $\mathbf{k}_\parallel$ is its component along the target surface.

The functions inside the layer, determined by the boundary conditions, can be written (for constant U) as

$$\psi^{(L,R)}(\mathbf{k},\nu) = e^{i\mathbf{k}_\parallel\mathbf{r}_\parallel}e^{-ik_\perp a/2}\times$$
$$\times\,\frac{t\gamma^{1/2}}{1-r^2\gamma^2}\sum_{\sigma=\pm1}A_\sigma^{(L,R)}e^{i\sigma\bar{k}z}. \tag{45}$$

Here $\bar{k}$ is the normal component of neutron momentum inside the target sample

$$\bar{k} = \sqrt{k_\perp^2 - k_0^2}, \quad k_0^2 = 4\pi\beta_c n, \tag{46}$$

where k_0 is the value of the neutron wave number $k_\perp$ at the barrier, r and t are the reflection and transition coefficients for the target surface

$$t = \frac{2k_\perp}{k_\perp + \bar{k}}, \quad r = \frac{k_\perp - \bar{k}}{k_\perp + \bar{k}}, \tag{47}$$

and the coefficients A are determined by

$$A_{+1}^{(L)} = 1, \quad A_{-1}^{(L)} = -r\gamma \quad, A_{+1}^{(R)} = -r\gamma, \quad A_{-1}^{(R)} = 1. \tag{48}$$

The factor

$$\gamma = e^{i\bar{k}a} \tag{49}$$

oscillates very rapidly as a function of $k_\perp$ above the barrier ($k_\perp > k_0$), and vanishes below the barrier ($k_\perp < k_0$).

Below we use the "left" solution (43) for the input channel function. Then, the output channels with the backward and forward scattering angles correspond to the "left", L, (43) and "right", R, (44) solutions, respectively. Inside the layer these solutions can be represented as

$$\bar{\psi}^{(L,R)}(\mathbf{k}',\nu) = e^{-i\mathbf{k}'_\parallel\mathbf{r}_\parallel}e^{-ik'_\perp a/2}\times$$
$$\times\,\frac{t'\gamma'^{1/2}}{1-r'^2\gamma'^2}\sum_{\sigma=\pm1}A_\sigma'^{(L,R)}e^{i\sigma\bar{k}'z}. \tag{50}$$

All momenta and momentum dependent quantities (46)-(49) for the output channel are denoted by primes: $k'_\perp$, $\bar{k}'$, t', r', A'_σ, γ'. They are interrelated by the same equations as that for the input channel.

Combining (45) and (50) we obtain for (7)

$$\mathbf{B}(\mathbf{q}) = i\beta_c tt'\frac{e^{-i(k_\perp+k'_\perp)a/2}}{(1-r^2\gamma^2)(1-r'^2\gamma'^2)}\Sigma_\parallel\boldsymbol{\Sigma}. \tag{51}$$

Here

$$\Sigma_\parallel = \sum_{\nu_\parallel}e^{i(\mathbf{Q}_\parallel-\mathbf{q}_\parallel)\mathbf{r}_\parallel}, \quad \mathbf{Q}_\parallel = \mathbf{k}_\parallel - \mathbf{k}'_\parallel, \tag{52}$$

and

$$\boldsymbol{\Sigma} = \sum_{\sigma,\sigma'}A_\sigma A'_{\sigma'}\left(\mathbf{Q}_\parallel + Q_\perp^{\sigma\sigma'}\mathbf{e}_z\right)\Sigma_\perp^{\sigma\sigma'}, \tag{53}$$

where

$$Q_\perp^{\sigma\sigma'} = \sigma\bar{k} + \sigma'\bar{k}', \quad \Sigma_\perp^{\sigma\sigma'} = (\gamma\gamma')^{1/2}\sum_{\nu_\perp}e^{i(Q_\perp^{\sigma\sigma'}-q_\perp)z}. \tag{54}$$

Summation over the nuclei on the plane parallel to the target surface gives

$$\Sigma_\parallel = (2\pi)^2 n_\parallel\sum_{\mathbf{G}_\parallel}\delta^{(2)}(\mathbf{Q}_\parallel - \mathbf{q}_\parallel - \mathbf{G}_\parallel), \tag{55}$$

where summation over the longitudinal reciprocal lattice vector $\mathbf{G}_\parallel$ arises for crystals, and $n_\parallel$ is the number of nuclei per the unit area of the fixed plane ($z = \text{const}$). Therefore we have the equality

$$\mathbf{Q}_\parallel = \mathbf{q}_\parallel + \mathbf{G}_\parallel \tag{56}$$

for the longitudinal transferred momentum.

The cross section (6) is proportional to the second power of the quantity $\Sigma_\parallel$. Then,

$$\left|\Sigma_\parallel\right|^2 = S(2\pi)^2 n_\parallel^2\sum_{\mathbf{G}_\parallel}\delta^{(2)}(\mathbf{Q}_\parallel - \mathbf{q}_\parallel - \mathbf{G}_\parallel), \tag{57}$$

where S is the surface area of the sample.

For a non-crystalline substance we replace summation over nuclear planes by integration

$$\Sigma_\perp^{\sigma\sigma'} = (\gamma\gamma')^{1/2} n_\perp \int\limits_{-a/2}^{a/2} e^{i(Q_\perp^{\sigma\sigma'}-q_\perp)z} dz \tag{58}$$

and obtain

$$\Sigma_\perp^{\sigma\sigma'} = (\gamma\gamma')^{1/2} n_\perp \Delta(q_\perp - Q_\perp^{\sigma\sigma'}), \tag{59}$$

where

$$\Delta(x) = \frac{2\sin(xa/2)}{x}. \tag{60}$$

Here $n_\perp$ is the number of nuclear planes per the unit length along the z axis ($n_\parallel n_\perp = n$). The function $\Delta(x)$ peaks sharply for small value of the argument.

For crystals the sum $\Sigma_\perp^{\sigma\sigma'}$ has additional peaks when $Q_\perp^{\sigma\sigma'} - q_\perp$ is close to the transverse reciprocal lattice vector $G_\perp$. In this case we take

$$\Sigma_\perp^{\sigma\sigma'} = (\gamma\gamma')^{1/2} n_\perp \Delta(q_\perp + G_\perp - Q_\perp^{\sigma\sigma'}), \tag{61}$$

assuming the argument in Δ-function is in the first Brillouin zone. Since the vector $q_\perp$ (originated from correlation function) is in the first Brillouin zone, the vector $G_\perp$ should compensate, if necessary, exceeding part of $Q_\perp^{\sigma\sigma'}$.

5 Inelastic cross section and inelastic transition probability

With the given correlation function (41) and quantity $\mathbf{B}$ (51), the general expression for the inelastic cross section (6) is fully defined and we can easily integrate over $\mathbf{q}_\parallel$ with the help of (57). Taking into account contributions from both, longitudinal and transverse parts of the correlation function, we find

$$\frac{d\sigma_{ie}^{l,t}}{d^3k'} = S\frac{\alpha n \beta_c^2 \hbar^2 n_0(\omega)}{2\pi k m M c_{l,t}^2} |t|^2 |t'|^2 \sum_{\mathbf{G}_\parallel} \Pi_{l,t}\,, \tag{62}$$

where the function

$$\begin{aligned} \Pi_{l,t} = {} & \frac{|\gamma|\,|\gamma'|}{|1-r^2\gamma^2|^2\,|1-r'^2\gamma'^2|^2} \times \\ & \times \sum_{\sigma,\sigma',\tau,\tau'} A_\sigma A_\tau^* A'_{\sigma'} A'^*_{\tau'}\, J_{l,t}(\lambda,\eta) \end{aligned} \tag{63}$$

includes all factors γ and γ' that are strongly oscillating above the barrier and exponentially small below it.

The factor $J_{l,t}(\lambda,\eta)$ depends on transverse momenta inside the target in combinations

$$\lambda = Q_\perp^{\sigma\sigma'} - G_\lambda, \quad \eta = Q_\perp^{\tau\tau'^*} - G_\eta, \tag{64}$$

where λ and η are assumed to be in the first Brillouin zone, and the difference from the full combinations $Q_\perp^{\sigma\sigma'}$ and $Q_\perp^{\tau\tau'^*}$ (see (54)) is compensated by the transverse components G_λ and G_η of the reciprocal lattice vectors. The factor $J_{l,t}(\lambda,\eta)$ is defined by the integral with the correlation function $\Omega_{l,t}$ and has a different form for the longitudinal and transverse cases,

$$J_{l,t}(\lambda,\eta) = \frac{1}{\pi}\int\limits_{-\infty}^{+\infty} dq_\perp \bar{\Omega}_{l,t}(q_\perp)\Delta(q_\perp-\lambda)\Delta(q_\perp-\eta)F_{l,t}(q_\perp), \tag{65}$$

where

$$F_l(q_\perp) = \frac{(\mathbf{Q}_\parallel\mathbf{q}_\parallel + Q_\perp^{\sigma\sigma'}q_\perp)(\mathbf{Q}_\parallel\mathbf{q}_\parallel + Q_\perp^{\tau\tau'^*}q_\perp)}{q_\parallel^2 + q_\perp^2}, \tag{66}$$

$$F_t(q_\perp) = Q_\parallel^2 + Q_\perp^{\sigma\sigma'}Q_\perp^{\tau\tau'^*} - F_l(q_\perp). \tag{67}$$

Note, that the functions $F_{l,t}(q_\perp)$, as well as $J_{l,t}$, depend on indices σ, σ', τ and τ', but, to simplify notations, we omit them. Here and below we use $\mathbf{q}_\parallel$, defined from (56)

$$\mathbf{q}_\parallel = \mathbf{Q}_\parallel - \mathbf{G}_\parallel, \tag{68}$$

as a fixed quantity. The correlation function $\bar{\Omega}(q_\perp)$, when parameterized as in (41) by Γ^2 and p^2, has a universal form for the longitudinal and transverse cases, and their specificity arises only from the numerical values of these parameters. Hence we shall omit the subscripts on $\bar{\Omega}(q_\perp)$ till the last, numerical stage.

The inelastic transition probability (8) with the use of (62) takes the form

$$\frac{dw_{l,t}(k_\perp,k_\parallel\to\varepsilon')}{d\varepsilon'} = \frac{\alpha\beta_c k\, n_0(\omega)}{Mc_{l,t}^2} W_{l,t}(k_\perp,k_\parallel\to\varepsilon'), \tag{69}$$

where the dimensionless factor W is given by

$$W_{l,t}(k_\perp,k_\parallel\to\varepsilon') = \frac{k_\perp}{\pi^2 k}\int\limits_0^{k'} dk'_\perp \int\limits_0^{\pi} d\varphi\, |t'|^2\, \Pi_{l,t}. \tag{70}$$

Here one integrates over $k'_\perp$ (up to $k' = \sqrt{2m\varepsilon'}/\hbar$) and φ, the angle between $\mathbf{k}'_\parallel$ and $\mathbf{k}_\parallel$, with fixed ε'.

For crystals, the final momentum $\mathbf{k}'$ is split by parts inside the first Brillouin zone, $\mathbf{k}'_1$, and $\mathbf{G}$. So the integral (8) over $\mathbf{k}'$ should be understood as that over $\mathbf{k}'_1$ and, if necessary, a sum over $\mathbf{G}$.

The detailed energy distribution inside a high Brillouin zone is of no interest, and we shall consider the full integrals over each zone, assuming that the final energy depends only on $\mathbf{G}$, $\varepsilon' \simeq \hbar^2 G^2/2m$. In analogy with (8), (69) and (70) we define transition probability per bounce

$$w_{l,t}(k_\perp,k_\parallel\to\mathbf{G}) = \frac{1}{S_\perp}\int \frac{d\sigma_{ie}^{l,t}}{d^3k'} d^3k', \tag{71}$$

which can be presented in the form

$$\begin{aligned} w_{l,t}(k_\perp, k_\parallel \to \mathbf{G}) = \frac{\alpha\beta_c k\, n_0(\hbar G^2/2m)}{M c_{l,t}^2} \times \\ \times \frac{\hbar^2 G^2}{2m}\, W_{l,t}(k_\perp, k_\parallel \to \mathbf{G}), \end{aligned} \tag{72}$$

where

$$W_{l,t}(k_\perp, k_\parallel \to \mathbf{G}) = \frac{k_\perp}{\pi^2 k G^2} \int d^3k'\, \Pi_{l,t}(\mathbf{G}) \tag{73}$$

is the dimensionless factor.

The transition probabilities (69) and (72) are quite general and fully defined but rather complicated even for numerical analysis. However, a drastic simplification can be achieved by analytic calculations even for the general case.

In our present publication we consider only a specific case that is when initial neutron energy is below the optical potential. Moreover, for the sake of simplicity in the main part of the paper we shall use only the results of the theoretical calculations referring to an Appendix, where the calculations are presented in details. Below we explain just the main steps of the solution.

First, in A.1 we calculate the integral (65). It turns out to be performed ”almost exactly” by transforming (65) into a contour integral in the complex $q_\perp$ plane with the use of the four-pole structure of the correlation function (41).

The next step, calculation of the sum in (63), is performed in A.2. Comparative importance of the 16 terms in the sum is very sensitive to the position of the initial and the final neutron energies. The result was obtained for the initial neutron energy below the barrier and for any final energy of the scattered neutron. After this stage, the inelastic cross section is defined as a function of final neutron momentum, $\mathbf{k}'$.

The last stage, integration over angular distribution of the scattered neutrons, is done in A.3 and A.4. Here the momentum transfer between the neutron and crystal lattice is very specific and has required a quite different approach (see A.4).

We write down the final results for the dimensionless quantities (70) and (73).

For transitions inside the first Brillouin zone ($\mathbf{G} = 0$) the factor (70) was found as

$$\begin{aligned} W_l(k_\perp, k_\parallel \to \varepsilon') = \frac{k_\perp f(k'_\perp) x_0}{3\pi k} + \\ + \frac{2k_\perp \Gamma^2 k'^2}{\pi k æ \left(k'^2 - \epsilon\,\omega^2/c_l^2\right)^{3/2}}, \end{aligned} \tag{74}$$

$$W_t(k_\perp, k_\parallel \to \varepsilon') = \frac{2k_\perp f(k'_\perp) x_0}{3\pi k}, \tag{75}$$

where

$$f(k'_\perp) = \begin{cases} 4k'_\perp/k_0^2, & k'_\perp < k_0, \\ 4/(k'_\perp + \sqrt{k'^2_\perp - k_0^2}\,), & k'_\perp > k_0, \end{cases} \tag{76}$$

with $k'_\perp = \sqrt{k'^2 - k_\parallel^2}$,

$$æ = \sqrt{k_0^2 - k_\perp^2}, \tag{77}$$

and

$$x_0(\omega) = \sqrt{\frac{\sqrt{(\epsilon\,\omega^2/c^2)^2 + \Gamma^4} + \epsilon\,\omega^2/c^2}{2}}. \tag{78}$$

The factors (73) for the case $\mathbf{G} \neq 0$ were reduced to

$$W_l(k_\perp, k_\parallel \to \mathbf{G}) = \frac{4k_\perp x_0}{3k æ}, \tag{79}$$

$$W_t(k_\perp, k_\parallel \to \mathbf{G}) = \frac{8k_\perp x_0}{3k æ}. \tag{80}$$

The transition probabilities (74), (75) and (79), (80) can be further simplified by averaging over the neutron incident angle. There are two factors with angular dependence in (74), (75) and (79), namely $k_\perp/(k\,æ)$ and $k_\perp f(k'_\perp)/k$. Following (16) we introduce

$$\langle \frac{k_\perp}{k æ} \rangle = \frac{1}{4k} A(\frac{\varepsilon}{U}), \tag{81}$$

where

$$A(x) = \frac{1}{x}\left(\arcsin\sqrt{x} - \sqrt{x(1-x)}\right), \tag{82}$$

and

$$\langle \frac{k_\perp f(k'_\perp)}{k} \rangle = \frac{1}{k} B(\frac{\varepsilon}{U}, \frac{\varepsilon'}{U}), \tag{83}$$

where the function $B(x, x')$ has a different form in three regions of the variables: $x' < 1$, $1 < x' < 1 + x$, $1 + x < x'$, and can be presented as

$$B(x, x') = C(x, \frac{x'}{x}) - C(x, \frac{x'-1}{x}), \tag{84}$$

with

$$C(x, y) = x \int\limits_{\min(0,y)}^{\min(1,y)} \sqrt{(1-z)(y-z)}\; dz. \tag{85}$$

Note the two simple limits

$$\begin{aligned} &B(x, x') \simeq x/2, && \text{for} \quad |x' - x| \ll 1, \\ &B(x, x') \simeq (1/3)\sqrt{x/x'}, && \text{for} \quad x' \gg 1. \end{aligned} \tag{86}$$

The final expressions for $W_{l,t}$, defined in (70) and (73), averaged over the angle of incidence, are of the form

$$\begin{aligned} W_l(\varepsilon \to \varepsilon') = \frac{x_0}{3\pi k} B(\frac{\varepsilon}{U}, \frac{\varepsilon'}{U}) + \\ + \frac{\Gamma^2 k'^2}{2\pi k \left(k'^2 - \epsilon\,\omega^2/c_l^2\right)^{3/2}} A(\frac{\varepsilon}{U}), \end{aligned} \tag{87}$$

$$W_t(\varepsilon \to \varepsilon') = \frac{2x_0}{3\pi k} B(\frac{\varepsilon}{U}, \frac{\varepsilon'}{U}), \tag{88}$$

$$W_l(\varepsilon \to \mathbf{G}) = \frac{x_0}{3k} A(\frac{\varepsilon}{U}), \quad W_t(\varepsilon \to \mathbf{G}) = \frac{2x_0}{3k} A(\frac{\varepsilon}{U}). \tag{89}$$

The second terms both in (74) and (87) are valid only for large energy transfer (see (199), (200) and text before).

6 Physical application. Specific ultracold neutron interaction with solids and liquids

In the previous section, specific cases of general equations were analyzed with the use of mathematical criteria. In this section, we consider the problems from a physical point of view, making classification by the relaxation processes, phonon-like or diffusion-like types, and the range of the energy transfer, with a special attention to the region of small heating and cooling, as well as to upscattering region. The substances under investigation are of crystalline, amorphous and liquid type, commonly used in experiments.

There are two longitudinal modes, phonon-like and thermo-diffusion, both for solids and liquids, and only one transverse mode. The latter is of the pure phonon type for solids, and of the combined type for liquids, that transforms from the diffusion type at small energy transfer to that of phonon type at large energy transfer (see Section 3).

6.1 Phonon-like mode, $\mathbf{G} = 0$

Phonon-like modes involve low damping, i.e. $\Gamma_p \to 0$. Therefore, one can neglect the last term in (87) and use for (78) $x_0(\omega) = |\omega|/c$. For solids, when $\mathbf{G} = 0$, the sum over longitudinal and transverse modes gives from (87) and (88)

$$\frac{dw_p(\varepsilon \to \varepsilon')}{d\varepsilon'} = \frac{\beta_c |\omega| n_0(\omega)}{\pi M c^3} B(\frac{\varepsilon}{U}, \frac{\varepsilon'}{U}), \tag{90}$$

where c is defined by

$$\frac{3}{c^3} = \frac{1}{c_l^3} + \frac{2}{c_t^3}. \tag{91}$$

For the low energy part of the spectrum one can use (23) and find

$$\frac{dw_p(\varepsilon \to \varepsilon')}{d\varepsilon'} = \frac{\beta_c k_T v_T}{2\pi M c^3} B(\frac{\varepsilon}{U}, \frac{\varepsilon'}{U}), \quad |\varepsilon' - \varepsilon| \ll T. \tag{92}$$

This part of the spectrum is completely determined by the function $B(x, x')$. Here and below we use the quantities

$$k_T = \frac{\sqrt{2mT}}{\hbar}, \quad v_T = \sqrt{\frac{2T}{m}}. \tag{93}$$

The contribution of inelastic processes with $\mathbf{G} = 0$ to the total probability of the UCN escape from the trap can be estimated by integration of (90) from the barrier U up to the Debye energy

$$\varepsilon_D = \hbar c (6\pi^2 n)^{1/3}. \tag{94}$$

Since $U \ll \varepsilon_D$, it gives

$$w_p(\varepsilon) = c_1(\frac{\varepsilon_D}{T}) \frac{\beta_c k_T}{12\pi} \frac{m}{M} \frac{v v_T^2}{c^3}, \tag{95}$$

where $v = \sqrt{2\varepsilon/m}$ is the initial neutron velocity, and

$$c_1(y) = \int\limits_0^y \frac{x^{1/2} dx}{e^x - 1} \underset{y \to \infty}{\longrightarrow} 2.315. \tag{96}$$

For liquids, the contribution of the longitudinal phonon-like mode is of the form (90), (92) and (95), where $1/c^3$ should be replaced by $1/3c_l^3$. The transverse mode for liquids is considered below (see Sec. 6.4).

6.2 Phonon upscattering, $\mathbf{G} \neq 0$

The main process for upscattering in crystals goes with momentum transfer from the lattice. Assuming $\Gamma_p \to 0$ and summing over longitudinal and transverse phonons, we obtain for the total upscattering probability from (72) and (89)

$$w_p^{up}(\varepsilon) = \frac{\beta_c \hbar^3}{4m^2 M c^3} A(\frac{\varepsilon}{U}) \sum_{\mathbf{G}_\parallel, G_\perp > 0} G^4 n_0(\frac{\hbar G^2}{2m}), \tag{97}$$

where c is given by (91). Restriction in the sum with $G_\perp > 0$ is made since the summation over backward and forward scattering was performed earlier.

To estimate the probability we replace summation over $G_\perp > 0$ and $\mathbf{G}_\parallel$ by integration

$$\sum_{\mathbf{G}_\parallel, G_\perp > 0} \quad \longrightarrow \quad \frac{1}{2} \int \frac{d^3 G}{(2\pi/a_0)^3}, \tag{98}$$

where $a_0 = \sqrt[3]{M/\rho}$ is the lattice constant. Integral over $\varepsilon' = \hbar^2 G^2 / 2m$ up to Debye energy gives

$$w_p^{up}(\varepsilon) = c_2(\frac{\varepsilon_D}{T}) \frac{\pi \beta_c k_T}{4} \left(\frac{a_0 k_T}{2\pi}\right)^3 \frac{m}{M} \left(\frac{v_T}{c}\right)^3 A(\frac{\varepsilon}{U}), \tag{99}$$

where

$$c_2(y) = \int\limits_0^y \frac{x^{5/2} dx}{e^x - 1} \underset{y \to \infty}{\longrightarrow} 3.745. \tag{100}$$

The high energy upscattering due to phonons at $\mathbf{G} \neq 0$, was considered earlier [15, 16] by other approaches. The probability (99) coincides with the result, presented, for example, in review paper [18].

6.3 Longitudinal thermo-diffusion mode, $\mathbf{G} = 0$

The differential probability of inelastic scattering via this mode, which follows from (69) and (87) with $\epsilon = 0$, can be presented in the form

$$\frac{dw_d(\varepsilon \to \varepsilon')}{d\varepsilon'} = \frac{\alpha \beta_c \Gamma_d n_0(\omega)}{3\sqrt{2}\,\pi M c_l^2} \left(B(\frac{\varepsilon}{U}, \frac{\varepsilon'}{U}) + \right. \\ \left. + \frac{3\hbar \Gamma_d}{2\sqrt{m\varepsilon'}} A(\frac{\varepsilon}{U})\, \theta(\varepsilon' - \varepsilon) \left(1 - e^{-\varepsilon'/10\varepsilon}\right) \right), \tag{101}$$

where the last term in (87), valid only for large energy transfer ($\varepsilon' \gg \varepsilon$), is written with factors $\theta(\varepsilon' - \varepsilon)$ and $(1 - e^{-\varepsilon'/10\varepsilon})$, which provide attenuation at small ε' ($\theta(x) = 0$ for $x < 0$ and $\theta(x) = 1$ for $x > 0$). The damping parameter, Γ_d^2, given in (34), can be presented as

$$\frac{\Gamma_d}{k} = \left(\frac{|\varepsilon' - \varepsilon|}{d_D \varepsilon}\right)^{1/2}, \tag{102}$$

where

$$d_D = \frac{2mD_S}{\hbar} \tag{103}$$

is the dimensionless thermo-diffusion coefficient.

For small energy transfer, $\varepsilon' \sim \varepsilon$, the dominating first term in (101) takes the form

$$\frac{dw_d(\varepsilon \to \varepsilon')}{d\varepsilon'} \simeq \frac{\alpha \beta_c k_T}{6\pi M c_l^2} \frac{v v_T}{v_0^2 \sqrt{2d_D}} \sqrt{\frac{\varepsilon}{|\varepsilon' - \varepsilon|}}, \tag{104}$$

where $v_0 = \sqrt{2U/m}$ is the barrier velocity. It is clear, that the divergence at $\varepsilon' \to \varepsilon$ is integrable. This result for longitudinal thermo-diffusion and for fixed components $k_\perp$ and $k_\|$ of the initial neutron momentum was obtained in [14].

For large energy transfer, the main contribution comes from the second term in (101). It should be remembered that diffusion modes appear in hydrodynamic approximation. So, the energy transfer via this mode has sense only inside the hydrodynamic region (31), where $|\omega| \ll c_l^2/D_S$. It gives the boundary for ε', where (101) is reasonable,

$$\varepsilon' \ll \varepsilon_d \equiv \frac{2mc_l^2}{d_D}. \tag{105}$$

If $\varepsilon_D < \varepsilon_d$, the integration can be performed up to the Debye energy. It gives

$$w_d(\varepsilon) = c_1(\frac{\varepsilon_D}{T}) \frac{\alpha \beta_c k_T}{4\pi d_D} \frac{m}{M} \left(\frac{v_T}{c_l}\right)^2 A(\frac{\varepsilon}{U}). \tag{106}$$

6.4 Transverse mode for liquids, $\mathbf{G} = 0$

Taking $\alpha = \epsilon = 1$ (see text after (41)), we get from (69) and (88) the differential probability of inelastic scattering

$$\frac{dw_t(\varepsilon \to \varepsilon')}{d\varepsilon'} = \frac{2\beta_c x_0(\omega) n_0(\omega)}{3\pi M c_t^2} B(\frac{\varepsilon}{U}, \frac{\varepsilon'}{U}), \tag{107}$$

where $x_0(\omega)$ is given by (78) with $c \to c_t$, while the damping factor $\Gamma^2 \to \Gamma_t^2$ is of the form (37).

Hydrodynamic region (38), $|\omega| \ll c_t^2/\nu$, corresponds to the final neutron energy

$$\varepsilon' \ll \varepsilon_\nu \equiv \frac{2mc_t^2}{d_\nu}, \tag{108}$$

where

$$d_\nu = \frac{2m\nu}{\hbar} \tag{109}$$

is the dimensionless viscosity. On the other hand, (108) means $\Gamma_t^2 = |\omega|/\nu \gg \omega^2/c_t^2$, which simplifies $x_0(\omega)$,

$$x_0(\omega) = \frac{\Gamma_t}{\sqrt{2}}. \tag{110}$$

In the region $\varepsilon' \sim \varepsilon$, (107) takes the form

$$\frac{dw_t(\varepsilon \to \varepsilon')}{d\varepsilon'} \simeq \frac{\beta_c k_T}{3\pi M c_t^2} \frac{v v_T}{v_0^2 \sqrt{2d_\nu}} \sqrt{\frac{\varepsilon}{|\varepsilon' - \varepsilon|}}, \tag{111}$$

similar to (104) for longitudinal thermo-diffusion.

Beyond the hydrodynamic region, i.e. for large energy transfer, we have

$$\Gamma_t^2 \ll \frac{\omega^2}{c_t^2} \quad \Longrightarrow \quad x_0(\omega) = \frac{|\omega|}{c_t}, \tag{112}$$

and (107) transforms into (90) for transverse phonon-like mode, where $1/c^3$ should be replaced by $2/3c_t^3$.

6.5 Relative contribution of phonons and thermo-diffusion to large energy transfer

Phonon contribution to large energy transfer essentially depends on momentum exchange with the lattice. The probability for upscattering with ($\mathbf{G} \neq 0$, (99)) and without ($\mathbf{G} = 0$, (95)) such exchange differ by the factor v/c ($\sim 10^{-3}$ for UCN). The physical reason is simple. Inelastic scattering can be visualized as an absorption by the neutron of a quantum from the media with the energy $\hbar\omega$ and momentum $\hbar q$. The requirement for energy and momentum conservation does not allow this process with "free" quanta. But for UCN the normal component of momentum is pure imaginary, $i\text{æ}$, and instead of a δ-function, as in (55) for $\mathbf{q}_\|$, one has from (58)–(60) for $q_\perp$

$$\Sigma_\perp^{1\sigma'} \sim \frac{e^{i(q_\perp + G_\perp - \sigma' \bar{k}')a/2}}{\text{æ} + i(q_\perp + G_\perp - \sigma' \bar{k}')}. \tag{113}$$

Integrals over $q_\perp$ with (113) are very sensitive to the minimum value of imaginary factor, $q_\perp + G_\perp - \sigma' \bar{k}'$, which may be reached in the allowed $q_\perp$ range. For sound-like excitations, a rough estimate gives

$$q = \frac{\omega}{c} \sim \frac{v'}{c} k' \ll k', \tag{114}$$

where v' and k' are the velocity and wave number of scattered neutron. It is evident, that the large factor $\sigma' k'$ in the denominator of (113) can be compensated only by $G_\perp$. Then (113) can result in the large factor $1/\text{æ}$, which is seen in (79), (80). With $G_\perp = 0$ one may expect, instead of $1/\text{æ}$, the factor $1/k'_\perp$, the result at least by the factor v/c smaller.

Note, that the factor $1/\text{æ}$ is of the scale of the UCN intrusion length into the wall of the trap. Therefore, it is natural that the inelastic scattering probability is proportional to 1/æ. Thus, the factor $1/k'_\perp$ instead of 1/æ points to substantial suppression of the large energy transfer by the phonon mode with $\mathbf{G} = 0$.

The thermo-diffusion mode can be also effective for the large energy transfer, but the physics is quite different. Parameters ω and q of "diffusion quanta" are not strongly coupled, as in the phonon case, (114). Even with ω fixed by the energy transfer, $q_\perp$ is still allowed to be varied up to $\sim k'$. Thus, (113) can reach 1/æ even for $\mathbf{G} = 0$. The result can be seen from the last term in (74). It vanishes in the limit $\Gamma \to 0$ (for phonons), but is proportional to 1/æ for thermo-diffusion and results in the probability for upscattering (106) which may be comparable to that for phonons with $\mathbf{G} \neq 0$, (99).

7 Results for two specific target samples

In previous section we have obtained analytic results for each type of relaxation modes. To get the physical result for a specific experiment, one should combine several analytic formulae with the relaxation modes and parameters appropriately chosen. To demonstrate this procedure and examine general trends of final results and their sensitivity to physical parameters, it is worthwhile to consider some specific examples.

We have chosen stainless steel (SS) and Fomblin fluid (FF), two materials which are often used in real experiments and, on the other hand, have quite different relaxation properties. Both materials are not of a simple structure, and we shall use for them simplified descriptions, which are specified below.

7.1 Parameters for stainless steel

The nuclei ^{56}Fe are the dominant ones in stainless steel. Thus, we take $A = 56$, where $A = M/m$ is the mass number of the scatterer. Then, $\rho = 7.8$ g/cm^3 and, therefore, $n = 8.4 \cdot 10^{22}$ cm^{-3} and $a_0 = 2.3 \cdot 10^{-8}$ cm. For the coherent scattering length we take $b_c = 0.87 \cdot 10^{-12}$ cm, which gives for the barrier energy $U = 192$ neV. Sound velocities at $T = 293$ K are equal to: $c_l = 5850$ m/sec and $c_t = 3230$ m/sec.

For the case of stainless steel one should consider contributions from longitudinal and transverse phonons and thermo-diffusion, the main part of the diffusion-like processes. For the latter we need $\alpha = C_P/C_V - 1$ and the thermo-diffusion coefficient D_S,

$$\alpha = \frac{TK\beta_P^2}{\rho C_P}, \quad D_S = \frac{æ}{\rho C_P}, \tag{115}$$

where $K = -V(\partial P/\partial V)$ is the volume elasticity, and $\beta_P = (\partial V/\partial T)_P/V$ is the thermal coefficient of volume expansion. The corresponding values at normal temperature $T = 293$ K are listed in Table 1 as well as the calculated quantities α, D_S, and dimensionless parameters d_D and d_ν.

7.2 Parameters for Fomblin fluid

Fomblin is a hydrogen-free fluorinated oil (it is known also as perfluropolyether). It is quite viscous at room temperature and used to cover the walls of UCN storage traps because of the small neutron absorption and upscattering rate. There are different modifications of Fomblin oil and not all of them are described in the literature in detail. Thus we use typical values for Fomblin parameters. In addition, we ignore complex structure of Fomblin molecules and are treating it as a sim ple liquid.

The stoichiometry is roughly C_3F_6O. Thus we assume that the ^{16}F nucleus dominates in the fluid and $A = 16$ is the mass number of scatterer. We take $\rho = 1.9$ g/cm^3, then $n = 7.15 \cdot 10^{22}$ cm^{-3}. For the coherent scattering length we use $b_c = 0.565 \cdot 10^{-12}$ cm, which gives $U = 106$ neV in accordance with experiment. For all temperatures we take fixed sound velocities: $c_l = 1900$ m/sec and $c_t = 1500$ m/sec.

Parameters K, β_P, C_P, æ, ν as well as the calculated α, D_s, and dimensionless quantities d_D and d_ν are presented in Table 1 for two temperatures: $T = 293$ K and 373 K. Among these parameters viscosity ν is the most sensitive to the temperature.

7.3 Numerical results

We have calculated the probability of inelastic scattering for UCN with initial energy near half of the barrier height, that is for $\varepsilon = 80$ neV for stainless steel and $\varepsilon = 40$ neV for Fomblin. Contributions of phonons and diffusion modes are shown separately. Results for the differential probability are presented on Figs. 1, 2 and 3.

Integral probabilities

$$w(\varepsilon_f) = \int_U^{\varepsilon_f} \frac{dw(\varepsilon \to \varepsilon')}{d\varepsilon'}\, d\varepsilon' \tag{116}$$

of transition to the interval $U < \varepsilon' < \varepsilon_f$ per bounce are shown on Figs. 4, 5 and 6. For Fomblin both differential and integral inelastic scattering probabilities are presented for two different temperatures: 293 K and 373 K.

Test calculations have been carried out starting from the exact expressions (69) and (70). Comparison with results from simplified analytic formulae has shown quite small deviations in the whole energy range. So, we present numerical results based on analytic formulae.

For stainless steel, the phonon contribution at $\mathbf{G} = 0$ was calculated from (90) and thermo-diffusion contribution – from (101). Results at $T = 293$ K are shown by solid and dashed lines, respectively, on Figs. 1 and 4. The final neutron energy for stainless steel is restricted from above by

Table 1: Parameters for stainless steel (SS) and Fomblin fluid (FF).

	T, K	K, Pa	β_P, K^{-1}	C_P, $\frac{\mathrm{J}}{\mathrm{g \cdot K}}$	æ, $\frac{\mathrm{W}}{\mathrm{m \cdot K}}$	ν, $\frac{\mathrm{cm}^2}{\mathrm{sec}}$	α	D_S, $\frac{\mathrm{cm}^2}{\mathrm{sec}}$	d_D	d_ν
SS	293	$170{\cdot}10^9$	$3.6{\cdot}10^{-5}$	0.45	80	0.01	0.018	$2.28{\cdot}10^{-1}$	717.5	31.5
FF	293	$3{\cdot}10^9$	$6{\cdot}10^{-4}$	1.0	0.2	1.40	0.167	$1.05{\cdot}10^{-3}$	3.30	4405.7
	373	$2{\cdot}10^9$	$7{\cdot}10^{-4}$	1.1	0.2	0.07	0.175	$0.96{\cdot}10^{-3}$	3.02	220.3

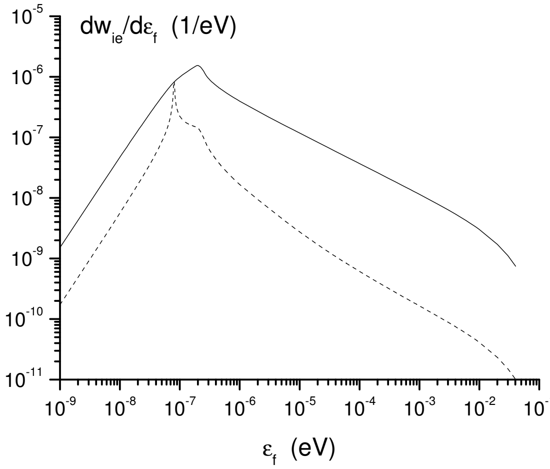

Figure 1: Inelastic scattering for UCN of 80 neV on stainless steel at $T = 293$ K: the differential probability $dw_{ie}/d\varepsilon_f$ per bounce as function of the final neutron energy ε_f. Solid line – phonon contribution, dashed line – thermo-diffusion contribution.

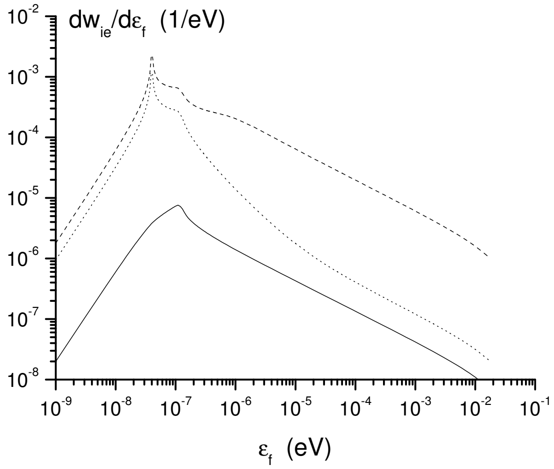

Figure 2: Inelastic scattering for UCN of 40 neV on Fomblin oil at $T = 293$ K: the differential probability $dw_{ie}/d\varepsilon_f$ per bounce as function of the final neutron energy ε_f. Solid line – longitudinal sound contribution, dotted line – transverse sound contribution, dashed line – thermo-diffusion contribution.

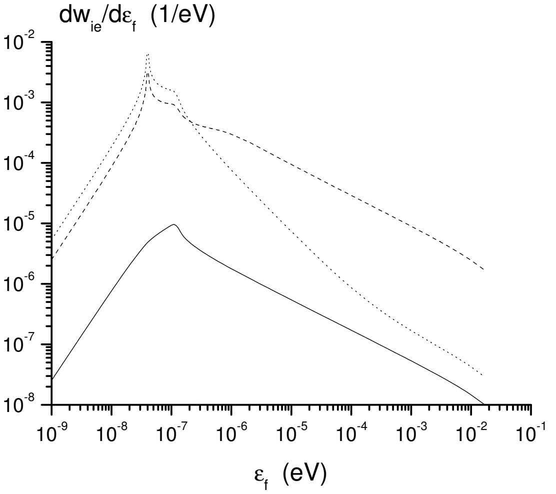

Figure 3: Inelastic scattering for UCN of 40 neV on Fomblin oil at $T = 373$ K: the differential probability $dw_{ie}/d\varepsilon_f$ per bounce as function of the final neutron energy ε_f. Solid line – longitudinal sound contribution, dotted line – transverse sound contribution, dashed line – thermo-diffusion contribution.

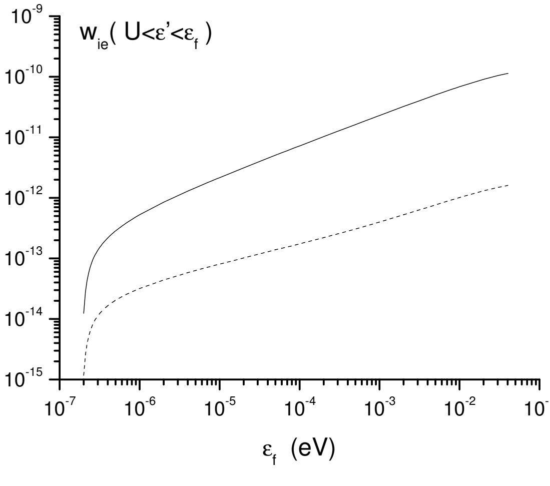

Figure 4: Inelastic scattering for UCN of 80 neV on stainless steel at $T = 293$ K: the integral probability w_{ie} per bounce of transition to the interval $U < \varepsilon < \varepsilon_f$ as function of ε_f. Solid line – phonon contribution, dashed line – thermo-diffusion contribution.

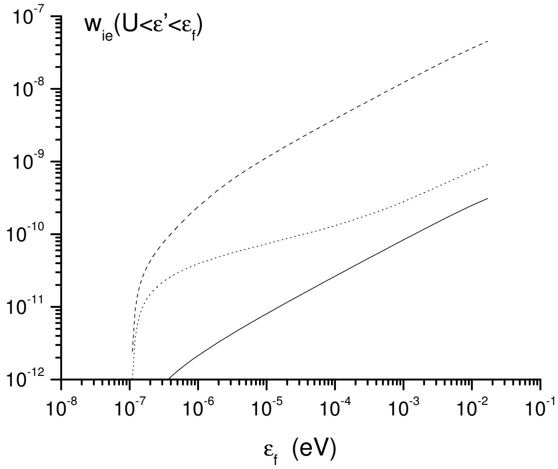

Figure 5: Inelastic scattering for UCN of 40 neV on Fomblin oil at $T = 293$ K: the integral probability w_{ie} per bounce of transition to the interval $U < \varepsilon < \varepsilon_f$ as function of ε_f. Solid line – longitudinal sound contribution, dotted line – transverse sound contribution, dashed line – thermo-diffusion contribution.

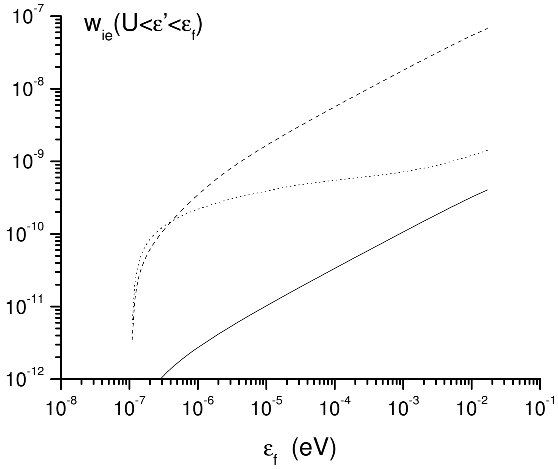

Figure 6: Inelastic scattering for UCN of 40 neV on Fomblin oil at $T = 373$ K: the integral probability w_{ie} per one bounce of transition to the interval $U < \varepsilon < \varepsilon_f$ as function of ε_f. Solid line – longitudinal sound contribution, dotted line – transverse sound contribution, dashed line – thermo-diffusion contribution.

the Debye energy $\varepsilon_D = 0.040$ eV (190) with sound velocity c from (91). The thermo-diffusion contribution should be restricted from above by the limit energy $\varepsilon_d = 0.001$ eV (see (105)).

Integral probabilities on Fig. 4, calculated for $\mathbf{G} = 0$, should be compared with the total upscattering probability at $\mathbf{G} \neq 0$, which is given by (99). At the temperature $T = 293$ K, it is equal to

$$w_p^{up} = 0.7 \cdot 10^{-6}. \tag{117}$$

For Fomblin, the longitudinal sound (phonon) contribution is given by (90) with $1/c^3 \to 1/3c_l^3$ (see the end of Sec. 6.1), the transverse sound contribution – by (107) and thermo-diffusion contribution – by (101). They were calculated both at $T = 293$ K and $T = 373$ K and are shown by solid, dotted and dashed lines, respectively, on Figs. 2, 3, 5 and 6. The final neutron energy is restricted from above by the Debye energy $\varepsilon_D = 0.017$ eV (190) with sound velocity from (91). For Fomblin, the energy $\varepsilon_d = 0.023$ eV (105), the limit for thermo-diffusion contribution, is greater than the Debye energy ε_D.

8 Discussion

Differential spectra (Figs. 1, 2 and 3) have well developed maxima for both modes, phonon (with $\mathbf{G} = 0$) and diffusion-like. For the phonon mode, the peak shape is determined by the function $B(\varepsilon/U, \varepsilon'/U)$. It has a maximum at $\varepsilon' = U$ ($\varepsilon < U$). In diffusion-like modes there is a divergence (integrable) at $\varepsilon' \simeq \varepsilon$ (see (104) and (111)). These general forms of the curves are the same for stainless steel and Fomblin, but the relative contribution from phonon-like and diffusion-like modes are quite different for the two substances. Contributions from phonons and diffusion into small energy transfer can be estimated from (92) and (104), (111). Omitting numerical factors, one has for diffusion-to-phonon contribution ratio

$$\frac{w_d}{w_p} \sim \frac{\alpha c}{v_0 \sqrt{d}}. \tag{118}$$

For thermo-diffusion, the high value of the ratio c/v_0 may be compensated by the smallness of the quantity $\alpha = C_P/C_V - 1$ and additionally suppressed by the factor $1/\sqrt{d_D}$, when d_D is large. This is just the case for stainless steel, when the right part of (118) is near unity. As for Fomblin, the right-hand side of (118) is near 40. This qualitative estimate agrees with numerical results presented on Figs. 1, 2 and 3. The thermo-diffusion contribution is comparable with the phonon one for stainless steel (Fig. 1) and dominates for Fomblin fluid (Figs. 2 and 3).

The transverse relaxation mode in liquids for small energy transfer is also of diffusion type, which originates from sound waves with high damping due to viscosity. The contribution of this mode, as compared to the longitudinal phonon one, can be evaluated from (118) with $\alpha = 1$. It far exceeds unity in agreement with Figs. 2 and 3.

It should be emphasized that the two diffusive modes, which, due to the large ratio (118), give the main contribution to the small energy transfer for Fomblin, are governed by different physical parameters. The transverse mode has no small parameter α, but its quantity $d \to d_\nu$ (109) differs from that for thermo-diffusion, d_D (103), by magnitude and temperature dependence (see Table 1).

Remark. The transverse mode was considered here with a simple liquid model (35)–(37), where transition to "ideal" liquid with very low viscosity is not correct. In this paper we have performed calculations for $d \geq 1$ (see Sec. A.3.1), so the definition (109) gives the lower bound for the viscosity ν. (In [14] we have argued, that for small $d < 1$ the contribution of diffusion mode to inelastic scattering vanishes.)

Let us now discuss quantitative results for the probability per bounce (116) for the neutron to change its energy from U up to $(10 - 10^3) \cdot U$, that is to go from ultra cold to very cold energy region ("small heating"). For stainless steel, the probability for neutron transition to the region from U to $(10 - 10^3) \cdot U$ is of the scale of $\sim 10^{-13} - 10^{-11}$ (Fig. 4), while for Fomblin it is of the scale of $\sim 10^{-10} - 10^{-9}$ (Figs. 5 and 6). Evidently, these contributions could not be seen in the measurements [5, 6, 7, 8, 9]. Nevertheless note, that our calculations for Fomblin shows a definit increase of low-energy heating with the temperature due to the contribution from diffusion-like transverse mode. It is in a qualitative agreement with the data [6, 9]. The measured effect of small heating on Fomblin seems to be explained by surface effects (see [8, 9]).

As a general conclusion, phonons are ineffective for small energy transfer both for stainless steel and Fomblin. Thermo-diffusion is even less effective for stainless steel, but gives very large effect (one-two orders of magnitude larger than phonons) for Fomblin, where the transverse diffusion mode gives comparable contribution and even exceeds thermo-diffusion when the temperature goes up. (Note, however, that it goes down more steeply when the transferred energy becomes higher.)

In the region of high energy transfer, the ratio of thermo-diffusion and phonon (at $\mathbf{G} = 0$) contributions can be estimated from (95) and (106),

$$\frac{w_d}{w_p} \sim \frac{\alpha c}{v_0 d_D}. \tag{119}$$

It is of the scale of 10^{-1} for stainless steel and 10^2 for Fomblin fluid. Thus, thermo-diffusion may dominate over phonons not only for small energy transfer, but as well for a large one, provided the dimensionless thermo-diffusion coefficient d_D is low. This conclusion may have sense only for liquids and amorphous materials, since for crystals, and stainless steel in particular, the main process for the transition up to the temperature region, upscattering, is that with momentum exchange with the lattice, $\mathbf{G} \neq 0$ (see Sec. 6.5).

Therefore, the processes responsible for high energy transfer are quite different for crystals and amorphous materials. Our result for coherent UCN upscattering on pure crystalline material (99) coincides with that previously obtained. It is known that its estimate (117) is one-two orders of magnitude too small to be observed in a real storage experiments. The reason is, evidently, a much higher absorption rate due to the radiative capture and possible upscattering on hydrogen contamination of the surface.

For Fomblin only the surface effects have been discussed in details so far. We have not found any published results with evaluation of escape probability from the bulk properties of this material. In other words, there is no understanding why the parameter f (see [10]) of bulk losses lies in the range 10^{-5} to 10^{-6}. Thus our result just for bulk effect given by the integral (116) (calculated with $\varepsilon_f = \varepsilon_D$) is new. Numerical results for Fomblin presented in Figs. 5 and 6 give for the loss probability per bounce ($\simeq f$) the following values: $0.5 \cdot 10^{-7}$ at 293 K and $0.7 \cdot 10^{-7}$ at 373 K. Possible reasons for the discrepancy of one-two orders of magnitude are mentioned in conclusion.

9 Conclusion and outlook

A theory for coherent inelastic scattering of ultracold neutrons was developed with a quite general form of the correlation function, which allows to consider energy-momentum exchange of the neutron with sound waves (phonons) as well as with diffusion-like relaxations. The latter appears when a correlation function is considered in the hydrodynamic region of momentum and energy transfers (the low limit for $\mathbf{q}$ and ω). Namely, we discussed the longitudinal thermo-diffusion mode both for solids and liquids as well as the diffusion-like transverse mode for liquids.

In the frame of this theory, we evaluated the probability per bounce for an ultracold neutron to gain energy and to go into cold or thermal region. In this paper the case $\mathbf{G} = 0$ (i.e. no momentum transfer between neutron and the crystal lattice) is consistently considered for the first time.

Numerical estimates are presented for the stainless steel storage bottle and one with Fomblin-fluid coated walls. For Fomblin, the most explored experimentally, theory predicts the overwhelming effect for thermo-diffusion processes, two-three orders of magnitude larger than from phonons, and a quite strong dependence on the temperature originated from viscosity. This result is in a qualitative agreement with experiments.

However, the numerical values for the upscattering probability per bounce obtained for stainless steel as well as for Fomblin are still one-two order of magnitude too small to fully explain experimental data. Thus, it is worthwhile to mention restrictions of the presented results and possible future improvements.

Results from diffusion processes are quite sensitive to the parameters of correlation function. It is very desirable to clarify the structure and parameters of correlation function, especially for liquids. In fact, it can be done by experiments in optics and other means outside the neutron physics.

We considered our samples as a spatially uniform media. This may not be correct for Fomblin, which exhibits some polymer features and may have a non-uniform structure at the scales comparable with the ultacold neutron reduced wave length ~ 10 nm. To get the correlation function for polymer and to include it in the neutron scattering theory is a serious problem for the future. Nevertheless, the effect may be evaluated from simple physical arguments. The probability for energy transfer, as was mentioned above, is proportional to the intrusion length or, what is the same, to the time of neutron-wall collision. Spatial polymer structure changes, in particular, the self-diffusion parameters for the neutron and increases the time, spent by the neutron inside the sample during the collision. This time can be evaluated from transmission experiments and the corresponding correction can be easily introduced into the formulae of this paper.

On the other hand, gigantic polymer molecules can behave as nano-particles. If it is the case, elastic scattering of the neutron by the whole moving molecule in their center-of-mass system would result in inelastic scattering of neutron in the laboratory system. Similar mechanism of small cooling and heating due to nano-particles at the surface of solid materials was proposed in [30].

No surface effect was included, which seems to be of no importance in solids for UCN large wave length. This argument may not concern specific surface excitations in liquids, say, capillary waves [22, 10], which can be included into consideration as one of the excitation modes. This particular case requires a different correlation function and is the subject for a separate paper.

Several important effects were not included in this paper. Among them are spin-flip effects and surface contamination with hydrogen etc. Note, for example, that in [4] evidences are presented that the total upscattering of UCN is mostly related just to hydrogen contamination of the walls of material traps. All these effects are of importance for incoherent scattering, not included in this paper, which deals only with coherent inelastic scattering of initially ultracold neutrons.

Acknowledgements

We are kindly grateful to V.I.Morozov, E.Korobkina and R.Golub for valuable discussions. The work was supported by RFBR grant 02-02-16808, grant NS-1885. 2003.2 and the program of bilateral cooperation between Russia and Germany, Grant No. RUS 02/030.

A Calculation of inelastic cross section and inelastic transition probability

The aim of this Appendix is to simplify the general expression (62)–(63) for inelastic cross section. The first stage is calculation of the integral (65).

A.1 Calculation of the integral $J_{l,t}(\lambda,\eta)$ (65)

We start with a general integral of the form

$$I(\lambda,\eta)=\frac{1}{\pi}\int\limits_{-\infty}^{+\infty} dq_\perp\,\Delta(q_\perp-\lambda)\Delta(q_\perp-\eta)\mathcal{F}(q_\perp), \tag{120}$$

where λ and η are complex parameters, and $\mathcal{F}(q_\perp)$ is a function with poles above ($q_{n\uparrow}$) and below ($q_{n\downarrow}$) the real axis, but not near it. The function $\Delta(x)$ is defined by (60), and therefore

$$\begin{aligned}\Delta(q_\perp-\lambda)\Delta(q_\perp-\eta)&=\frac{1}{(q_\perp-\lambda)(q_\perp-\eta)}\times\\ \times\left(2\cos\frac{(\lambda-\eta)a}{2}\right.&\left.-e^{i\left(q_\perp-\frac{\lambda+\eta}{2}\right)a}-e^{-i\left(q_\perp-\frac{\lambda+\eta}{2}\right)a}\right).\end{aligned} \tag{121}$$

We transform (120) into the contour integral closing a path in the upper or the lower half-plane. Then, neglecting the term proportional to $e^{-\operatorname{Im} q_{n\uparrow}a}$ and $e^{-|\operatorname{Im} q_{n\downarrow}|a}$, we get for any positions of λ and η

$$\begin{aligned}I(\lambda,\eta)=&\frac{2\sin(\lambda-\eta)a/2}{\lambda-\eta}\left(\mathcal{F}(\lambda)+\mathcal{F}(\eta)\right)\\ &+\frac{2\cos(\lambda-\eta)a/2}{\lambda-\eta}\left(\mathcal{P}(\lambda)-\mathcal{P}(\eta)\right),\end{aligned} \tag{122}$$

where the function $\mathcal{P}(\lambda)$ is defined by the residues in poles of $\mathcal{F}(q_\perp)$

$$\mathcal{P}(\lambda)=-i\left(\sum_{n\uparrow}\frac{\operatorname{res}_{n\uparrow}\mathcal{F}}{\lambda-q_{n\uparrow}}-\sum_{n\downarrow}\frac{\operatorname{res}_{n\downarrow}\mathcal{F}}{\lambda-q_{n\downarrow}}\right). \tag{123}$$

To apply the results for (65), one needs to specify the pole structure of the integrand. For the factors $F_{l,t}(q_\perp)$, it is evident from (66) and (67). The function $\bar{\Omega}_{l,t}(q_\perp)$ is given by (41) and can be presented as the sum of four simple pole terms. The poles are located symmetrically with respect to the axes at the points $x\pm iy$ and $-x\pm iy$, where

$$x=\sqrt{\frac{\sqrt{p^4+\Gamma^4}-p^2}{2}},\quad y=\sqrt{\frac{\sqrt{p^4+\Gamma^4}+p^2}{2}} \tag{124}$$

are real and positive. The function $\bar{\Omega}(q_\perp)$ takes the form

$$\bar{\Omega}(q_\perp)=\frac{1}{4i|z|^2}\left(U(q_\perp,z^*)-U(q_\perp,z)\right), \tag{125}$$

where $z=x+iy$ and

$$U(\alpha,z)=\frac{z}{\alpha-z^*}+\frac{z^*}{\alpha+z}. \tag{126}$$

This complex function of two complex variables will be extensively used below and it is worthwhile to exhibit its symmetry

$$U(\alpha,z)=U(-\alpha,-z)=-U(-\alpha,z^*)=U^*(\alpha^*,z^*). \tag{127}$$

The real and imaginary parts of this function for the first argument $\beta+i\gamma$ are of the form

$$\operatorname{Re}U(\beta+i\gamma,z)=\frac{2\beta x}{\Delta}\left(\beta^2+(\gamma+2y)^2-|z|^2\right), \tag{128}$$

$$\operatorname{Im}U(\beta+i\gamma,z)=-\frac{2x}{\Delta}\left(\beta^2\gamma+(\gamma+2y)(x^2+(\gamma+y)^2)\right), \tag{129}$$

where

$$\Delta=\left(\beta^2+x^2+(\gamma+y)^2\right)^2-4\beta^2x^2. \tag{130}$$

Note, that $U(i\gamma,z)$ is pure imaginary and given by

$$\operatorname{Im}U(i\gamma,z)=-\frac{2x(\gamma+2y)}{x^2+(\gamma+y)^2}. \tag{131}$$

Now, we are ready to apply the general result (122) and (123) to the integral (65). It is enough to find three "elementary" integrals $I_n(\lambda,\eta)$ $(n=1,2,3)$ with

$$\begin{aligned}\mathcal{F}_1(q_\perp)&=\bar{\Omega}(q_\perp),\\ \mathcal{F}_2(q_\perp)&=\frac{\bar{\Omega}(q_\perp)}{q_\parallel^2+q_\perp^2},\\ \mathcal{F}_3(q_\perp)&=\frac{q_\perp\bar{\Omega}(q_\perp)}{q_\parallel^2+q_\perp^2}.\end{aligned} \tag{132}$$

All $\mathcal{F}_n(q_\perp)$ have the poles from $\bar{\Omega}(q_\perp)$, the last two have the additional poles in $q_\perp=\pm iq_\parallel$. The functions $\mathcal{P}_n(\lambda)$ take the form

$$\begin{aligned}\mathcal{P}_1(\lambda)&=-\frac{1}{4|z|^2}\left(U(\lambda,z^*)+U(\lambda,z)\right),\\ \mathcal{P}_2(\lambda)&=\frac{\mathcal{P}_1(\lambda)}{q_\parallel^2+\lambda^2}-\frac{i\lambda U(iq_\parallel,z)}{2q_\parallel|z|^2(q_\parallel^2+\lambda^2)},\\ \mathcal{P}_3(\lambda)&=\frac{\lambda\mathcal{P}_1(\lambda)}{q_\parallel^2+\lambda^2}+\frac{iq_\parallel U(iq_\parallel,z)}{2|z|^2(q_\parallel^2+\lambda^2)}.\end{aligned} \tag{133}$$

Note, that $\mathcal{F}_n$ and $\mathcal{P}_n$, which determine $I_n(\lambda,\eta)$ by (122), contain the function $U(\alpha,z)$ (126) varied by first argument.

The function $J(\lambda,\eta)$ (65) can be presented as a sum of $I_n(\lambda,\eta)$ with coefficients evident from (66) and (67). After some rearrangement the results can be written in the form

$$J_{l,t}(\lambda,\eta) = J^{(1)}_{l,t}(\lambda,\eta) + J^{(2)}_{l,t}(\lambda,\eta). \tag{134}$$

Both terms in the right-hand side are proportional to the factors $U(\alpha,\beta)$, however, $J^{(1)}$ includes all terms with $\alpha=\lambda$ or η, while $J^{(2)}$ includes terms with $\alpha = iq_{\parallel}$. Namely,

$$J^{(1)}_{l,t}(\lambda,\eta) = \frac{e^{-i\frac{(\lambda-\eta)a}{2}}\Lambda_{l,t}(\lambda,\eta) - e^{i\frac{(\lambda-\eta)a}{2}}\Lambda_{l,t}(\eta,\lambda)}{\lambda-\eta}, \tag{135}$$

$$J^{(2)}_{l,t}(\lambda,\eta) = \cos\frac{(\lambda-\eta)a}{2}\,\Phi_{l,t}(\lambda,\eta)\,\frac{\operatorname{Im}U(iq_{\parallel},z)}{q_{\parallel}|z|^2}, \tag{136}$$

where

$$\Lambda_{l,t}(\lambda,\eta) = -\frac{F_{l,t}(\lambda)U(\lambda,z) - F_{l,t}(\eta)U(\eta,z^*)}{2|z|^2}, \tag{137}$$

$$\begin{aligned}\Phi_{l,t}(\lambda,\eta) = \pm&\frac{1}{(q_{\parallel}^2+\lambda^2)(q_{\parallel}^2+\eta^2)}\times\\ &\times\Big(q_{\parallel}^2(\mathbf{Q}_{\parallel}\mathbf{q}_{\parallel}+\lambda Q_{\perp}^{\sigma\sigma'})(\mathbf{Q}_{\parallel}\mathbf{q}_{\parallel}+\eta Q_{\perp}^{\tau\tau'^*}) -\\ &-(\lambda\mathbf{Q}_{\parallel}\mathbf{q}_{\parallel} - Q_{\perp}^{\sigma\sigma'}q_{\parallel}^2)(\eta\mathbf{Q}_{\parallel}\mathbf{q}_{\parallel} - Q_{\perp}^{\tau\tau'^*}q_{\parallel}^2)\Big),\end{aligned} \tag{138}$$

and the functions $F_{l,t}$ are given by (66) and (67). In (138) "+" and "-" correspond to "l" and "t", respectively.

Note, that the dependence on the parameter a, the thickness of the layer, is explicitly indicated in (135) and (136). All other functions are independent on a. The functions F and Φ are constructed entirely from kinematic factors, initial and final neutron momenta. Parameters of correlation function, $z = x+iy$, apart from the explicit factor $|z|^2$, enter only in the function $U(\alpha,z)$ with $\alpha = \lambda,\eta$ or $iq_{\parallel}$.

The cross section (62), (63) is the function of the incoming and outcoming neutron wave vectors, which are included in parameters $\mathbf{Q}_{\parallel} = \mathbf{k}_{\parallel} - \mathbf{k}'_{\parallel}$ (52) and $Q_{\perp}^{\sigma\sigma'}$, $Q_{\perp}^{\tau\tau'}$ (54). For the crystal these parameters are split into the parts inside the first Brillouin zone, $\mathbf{q}_{\parallel}$, λ, η, and corresponding reciprocal lattice vectors $\mathbf{G}_{\parallel}$, G_λ, G_η. Note, that

$$F_l(\lambda) = F_l(\eta) = Q_{\parallel}^2 + Q_{\perp}^{\sigma\sigma'}Q_{\perp}^{\tau\tau'^*}, \tag{139}$$

$$F_t(\lambda) = F_t(\eta) = 0, \quad \Phi_{l,t}(\lambda,\eta) = \pm Q_{\parallel}^2, \tag{140}$$

when all $\mathbf{G}_{\parallel}$, G_λ, G_η are zero.

Thus, with calculated $J(\lambda,\eta)$, the general expression for the inelastic cross section is of the form (62), (63) as the sum over the indices σ, σ', τ, τ'. This summation, for a general case, is cumbersome because the variables λ and η (64) enter the functions $U(\lambda,z)$ and $U(\eta,z)$ in a sophisticated way.

A.2 Inelastic cross section for initial sub-barrier neutrons

In this part of Appendix we specify the general expression for the inelastic cross section (62), (63) for the case, when the initial neutron is sub-barrier. The final energy can be both below and above the barrier. The scheme of approximation varies for these two cases, and they will be considered separately. The object of analysis will be the factor $\Pi_{l,t}$ in the cross section (62). All other factors are universal and will be added afterwards.

For the initial sub-barrier neutron it is useful to define

$$\bar{k} = i\text{æ}, \quad \text{æ} = \sqrt{k_0^2 - k_{\perp}^2}. \tag{141}$$

The quantity $\gamma = e^{-\text{æ}a} \to 0$ for the initial channel may be neglected everywhere. In particular, for the neutron coming from the left we have

$$A^{(L)}_{+1} = 1, \quad A^{(L)}_{-1} = -r\gamma \to 0. \tag{142}$$

To compensate γ in the first factor in (63) we need from the sum $\gamma^{-1} = e^{\text{æ}a}$. Therefore, the factor needed comes only from the first exponent in (135) with $\sigma=\tau=1$. The same exponent should be taken into account in (136).

Following (134), the Π factor (63) can be presented as the sum of two terms

$$\begin{aligned}\Pi^{(1)}_{l,t} = &\frac{|\gamma'|}{|1-r'^2\gamma'^2|^2}\sum_{\sigma',\tau'}A'_{\sigma'}A'^*_{\tau'}\times\\ &\times(\gamma')^{-\sigma'/2}(\gamma'^*)^{-\tau'/2}\,\frac{\Lambda^{\sigma'\tau'}_{l,t}(\lambda,\eta)}{\lambda-\eta},\end{aligned} \tag{143}$$

$$\begin{aligned}\Pi^{(2)}_{l,t} = &\frac{|\gamma'|}{|1-r'^2\gamma'^2|^2}\,\frac{\operatorname{Im}U(iq_{\parallel},z)}{2q_{\parallel}|z|^2}\sum_{\sigma',\tau'}A'_{\sigma'}A'^*_{\tau'}\times\\ &\times(\gamma')^{-\sigma'/2}(\gamma'^*)^{-\tau'/2}\,\Phi^{\sigma'\tau'}_{l,t}(\lambda,\eta).\end{aligned} \tag{144}$$

Parameters λ and η are defined by (64) and can be rewritten now as

$$\lambda = i\text{æ} + \sigma'\bar{k}'_1, \quad \eta = -i\text{æ} + \tau'\bar{k}'^*_1, \tag{145}$$

where $\bar{k}'_1 = \bar{k}' - G_{\perp}$ is the part of $\bar{k}'$ in the first Brillouin zone ($G_{\perp} = \sigma' G_\lambda = \tau' G_\eta$). The identity $e^{iG_{\perp}a} = 1$ for the reciprocal lattice vector is taken into account. The functions Λ and Φ in (143) and (144) depend on indices σ' and τ' via their arguments.

A.2.1 Final state: below the barrier

To be more precise, only normal to the surface component of the final neutron energy should be below the barrier. For the normal component of the final neutron wave vector inside the sample we introduce (with analogy to (141))

$$\bar{k}' = i\text{æ}', \quad \text{æ}' = \sqrt{k_0^2 - k'^2_{\perp}}. \tag{146}$$

In the sums (143), (144) over σ' and τ' the main term corresponds evidently to $\sigma' = \tau' = 1$ because the others contain the factor $\gamma' = e^{-\ae' a}$, which may be neglected apart from a small vicinity of the barrier, where $k'_\perp \to k_0$, $\ae' a \leq 1$ and γ' may approach the unity. The barrier region is discussed in details later. Note that even for $\sigma' = \tau' = 1$ only the coefficients $A'^{(L)}$ contribute to (143), (144), but not $A'^{(R)}$. Surely, it means that the neutrons coming from the left are scattered also to the left.

For the small energy transfer one may put $\mathbf{G}_\parallel = 0$ and $G_\lambda = G_\eta = 0$. Taking into account (139) and (140), we get

$$\Pi_l^{(1)} = \frac{\Lambda_l^{11}(\lambda_0, \lambda_0^*)}{2\lambda_0} = -\frac{(Q_\parallel^2 + |\lambda_0|^2)\,\mathrm{Im}\,U(\lambda_0, z)}{2|\lambda_0||z|^2},$$

$$\Pi_t^{(1)} = 0, \tag{147}$$

$$\Pi_{l,t}^{(2)} = \Phi_{l,t}^{11}(\lambda_0, \lambda_0^*)\,\frac{\mathrm{Im}\,U(iQ_\parallel, z)}{2Q_\parallel |z|^2} = \pm \frac{Q_\parallel\,\mathrm{Im}\,U(iQ_\parallel, z)}{2|z|^2}, \tag{148}$$

where

$$\lambda_0 = i(\ae + \ae'). \tag{149}$$

Note, that for pure imaginary first argument $\alpha = i\gamma$ the function $\mathrm{Im}\,U$ is given by (131).

A.2.2 Final state: above the barrier

In the sums (143), (144) over σ' and τ' all terms should be considered equally important, since $\gamma' = e^{i\bar{k}' a}$ is now not a small parameter. If we neglect radiative capture, then the quantities $\bar{k}'$ and r' are real, and $|\gamma'| = 1$.

It is useful to split (143), (144) into the sums with $\sigma' = \tau'$ (where $\eta = \lambda^*$) and that with $\sigma' = -\tau'$ (where $\eta = -\lambda$)

$$\Pi_{l,t}^{(1)} = \frac{1}{|1 - r'^2\gamma'^2|^2}\left(\sum_{\sigma'} |A'_{\sigma'}|^2 \frac{\Lambda_{l,t}^{\sigma'\sigma'}(\lambda, \lambda^*)}{2i\ae} + \right.$$
$$\left. + \sum_{\sigma'} A'_{\sigma'} A'^*_{-\sigma'} (\gamma')^{-\sigma'} \frac{\Lambda_{l,t}^{\sigma'\,-\sigma'}(\lambda, -\lambda)}{2\lambda}\right), \tag{150}$$

$$\Pi_{l,t}^{(2)} = \frac{\mathrm{Im}\,U(iq_\parallel, z)}{2q_\parallel |z|^2 |1 - r'^2\gamma'^2|^2}\left(\sum_{\sigma'} |A'_{\sigma'}|^2 \Phi_{l,t}^{\sigma'\sigma'}(\lambda, \lambda^*) + \right.$$
$$\left. + \sum_{\sigma'} A'_{\sigma'} A'^*_{-\sigma'} (\gamma')^{-\sigma'} \Phi_{l,t}^{\sigma'\,-\sigma'}(\lambda, -\lambda)\right). \tag{151}$$

For the explicit summation in (150) we need to know how $\Lambda_{l,t}^{\sigma'\sigma'}(\lambda, \lambda^*)$ and $\Lambda_{l,t}^{\sigma'\,-\sigma'}(\lambda, -\lambda)$ depend on σ'. From (137) with the use of symmetry properties (127) one can show that the quantity

$$\Lambda_{l,t}^{11}(\lambda, \lambda^*) \equiv \Lambda_{l,t}^{11}(\lambda_0, \lambda_0^*) \tag{152}$$

is pure imaginary, where

$$\lambda_0 = i\ae + \bar{k}'_1. \tag{153}$$

On the other hand

$$\Lambda_{l,t}^{-1\,-1}(\lambda, \lambda^*) \equiv \Lambda_{l,t}^{-1\,-1}(-\lambda_0^*, -\lambda_0) = \Lambda_{l,t}^{11}(\lambda_0, \lambda_0^*), \tag{154}$$

and

$$\Lambda_{l,t}^{1\,-1}(\lambda, -\lambda) \equiv \Lambda_{l,t}^{1\,-1}(\lambda_0, -\lambda_0),$$

$$\Lambda_{l,t}^{-1\,1}(\lambda, -\lambda) \equiv \Lambda_{l,t}^{-1\,1}(-\lambda_0^*, \lambda_0^*) = -\Lambda_{l,t}^{1\,-1\,*}(\lambda_0, -\lambda_0). \tag{155}$$

With the help of (152)–(155) one readily finds

$$\Pi_{l,t}^{(1)} = \frac{1}{|1 - r'^2\gamma'^2|^2}\left((1 + r'^2)\frac{\mathrm{Im}\,\Lambda_{l,t}^{11}(\lambda_0, \lambda_0^*)}{2\ae} + \right.$$
$$\left. + 2\mathrm{Re}\left(A'_{+1} A'^*_{-1} (\gamma')^{-1} \frac{\Lambda_{l,t}^{1\,-1}(\lambda_0, -\lambda_0)}{2\lambda_0}\right)\right). \tag{156}$$

The sum (151) in a similar way results in

$$\Pi_{l,t}^{(2)} = \frac{\mathrm{Im}\,U(iq_\parallel, z)}{2q_\parallel |z|^2 |1 - r'^2\gamma'^2|^2}\Big((1 + r'^2)\Phi_{l,t}^{11}(\lambda_0, \lambda_0^*) + $$
$$+ 2\mathrm{Re}\left(A'_{+1} A'^*_{-1} (\gamma')^{-1} \Phi_{l,t}^{1\,-1}(\lambda_0, -\lambda_0)\right)\Big), \tag{157}$$

where the quantity $\Phi_{l,t}^{11}(\lambda_0, \lambda_0^*)$ (138) is real.

The last terms in (156) and (157) have different values for backward (B) and forward (F) scattering because

$$\left[A'_{+1} A'^*_{-1} (\gamma')^{-1}\right]^B = A'^{(L)}_{+1} A'^{(L)*}_{-1} (\gamma')^{-1} = -r'(\gamma')^{-2}, \tag{158}$$

$$\left[A'_{+1} A'^*_{-1} (\gamma')^{-1}\right]^F = A'^{(R)}_{+1} A'^{(R)*}_{-1} (\gamma')^{-1} = -r'. \tag{159}$$

A.2.3 Final state: near the barrier. Resonances of penetration

With the results of two previous subsections we are able to consider the upscattering of UCN into the regions close to the barrier, below or above.

In the low vicinity of the barrier $\ae' \ll \ae$. Above the barrier two ”vicinities” should be distinguished, ”wide vicinity”, where $\bar{k}' \ll k_\perp$, but $\bar{k}' a \gg 1$, and ”close vicinity”, where $\bar{k}' a \leq 1$.

In the ”wide vicinity” of the barrier, $\ae'$ and $\bar{k}'$ may be treated as small parameters. Due to small energy transfer, we take $G_\lambda = G_\eta = 0$. In the approximation $\lambda \simeq \lambda_0 = i\ae$ and $\eta \simeq \lambda_0^*$ the equations (143) and (144) can be written as

$$\Pi_{l,t}^{(1)} \simeq \Xi(r', \gamma')\,\frac{\Lambda_{l,t}^{11}(\lambda_0, \lambda_0^*)}{2i\ae}, \tag{160}$$

$$\Pi_{l,t}^{(2)} \simeq \Xi(r', \gamma')\Phi_{l,t}^{11}(\lambda_0, \lambda_0^*)\,\frac{\mathrm{Im}\,U(iQ_\parallel, z)}{2Q_\parallel |z|^2}, \tag{161}$$

where the factor

$$\Xi(r', \gamma') = \frac{|\gamma'|}{|1 - r'^2\gamma'^2|^2} \sum_{\sigma', \tau'} A'_{\sigma'} A'^*_{\tau'} (\gamma')^{-\sigma'/2} (\gamma'^*)^{-\tau'/2} \tag{162}$$

for backward and forward scattering is equal to

$$\Xi^B(r',\gamma') = \frac{|1-r'\gamma'^2|^2}{|1-r'^2\gamma'^2|^2}, \quad \Xi^F(r',\gamma') = \frac{|\gamma'|^2\,|1-r'|^2}{|1-r'^2\gamma'^2|^2}. \tag{163}$$

When the final momentum $\bar{k}'$ is just above the barrier, where it is reasonable to put $r' \simeq 1$, then $\Xi^B \to 1$ and $\Xi^F \to 0$, and the corresponding barrier values of $\Pi_{l,t}$ (160) and (161) coincide with that from (147) and (148). The deviations arise only close to the points where

$$\gamma'^2 = e^{2i\bar{k}'a} = 1 \quad \Longrightarrow \quad \bar{k}'a = \pi n, \quad n = 1,2,3\ldots \tag{164}$$

and, therefore, a difference between r' and 1 is of importance. For these energies Π^B decreases and Π^F increases up to the peak values

$$\Pi^{(1)B,F}_{l,t} \simeq \frac{1}{4}\,\frac{\Lambda^{11}_{l,t}(\lambda_0,\lambda_0^*)}{2i\text{æ}}, \tag{165}$$

$$\Pi^{(2)B,F}_{l,t} \simeq \frac{1}{4}\,\Phi^{11}_{l,t}(\lambda_0,\lambda_0^*)\,\frac{\operatorname{Im} U(iQ_\parallel, z)}{2Q_\parallel |z|^2}. \tag{166}$$

It is seen from (164) that these minima in Π^B and maxima in Π^F arise when the thickness of the layer is divisible by the half of the neutron wave length in the substance. Thus, the reason for the oscillation of the cross section is the resonances of penetration through the layer.

When the final momentum is not too close to the barrier, the factors containing $\gamma' = e^{i\bar{k}'a}$ (e.g. $\left|1-r'^2\gamma'^2\right|^{-2}$) strongly oscillate. With increase of the neutron final energy the amplitude of oscillations goes down because $r' \to 0$. However, in the "wide vicinity" of the barrier the oscillations are of importance. For not very thin sample these oscillations cannot be resolved and only the smoothed cross section is of interest.

A.2.4 Smoothing over oscillations

The functions Π (156) and (157) with account for (158) and (159) oscillate due to the factors

$$\begin{aligned} \frac{1}{|1-r'^2\gamma'^2|^2} &= \sum_{l,m=0}^{\infty} r'^{2(l+m)}\, e^{2i(l-m)\bar{k}'a}, \\ \frac{(\gamma')^{-2}}{|1-r'^2\gamma'^2|^2} &= \sum_{l,m=0}^{\infty} r'^{2(l+m)}\, e^{2i(l-m-1)\bar{k}'a}. \end{aligned} \tag{167}$$

Keeping only the terms with zero indices in the exponents, we get the smoothed functions

$$\begin{aligned} \langle \Pi^{(1)B,F}_{l,t} \rangle = \frac{1}{1-r'^4} \Bigg(&(1+r'^2)\frac{\operatorname{Im}\Lambda^{11}_{l,t}(\lambda_0,\lambda_0^*)}{2\text{æ}} - \\ &-2r'^n \operatorname{Re}\frac{\Lambda^{1\,-1}_{l,t}(\lambda_0,-\lambda_0)}{2\lambda_0} \Bigg), \end{aligned} \tag{168}$$

$$\begin{aligned} \langle \Pi^{(2)B,F}_{l,t} \rangle = \frac{\operatorname{Im} U(iq_\parallel, z)}{2q_\parallel |z|^2 (1-r'^4)} \Big(&(1+r'^2)\Phi^{11}_{l,t}(\lambda_0,\lambda_0^*) - \\ &- 2r'^n \operatorname{Re}\Phi^{1\,-1}_{l,t}(\lambda_0,-\lambda_0) \Big), \end{aligned} \tag{169}$$

where $n = 3$ for backward and $n = 1$ for forward scattering, and λ_0 is given by (153).

The smoothing is not justified in the "close vicinity" of the barrier where $\bar{k}'a \sim 1$. But since the smoothed quantities (168) and (169) have the same limiting values as (160) and (161), one may use the smoothed cross section everywhere above the barrier.

The functions $\Lambda_{l,t}$, which enter (168), are disclosed from (137), (66) and (67) as

$$\begin{aligned} &\operatorname{Im}\Lambda^{11}_{l}(\lambda_0,\lambda_0^*) = \\ &= -\operatorname{Im}\left(\frac{(\mathbf{Q}_\parallel \mathbf{q}_\parallel + Q^{11}_\perp \lambda_0)(\mathbf{Q}_\parallel \mathbf{q}_\parallel + Q^{11\,*}_\perp \lambda_0)\, U(\lambda_0, z)}{|z|^2 (q_\parallel^2 + \lambda_0^2)} \right), \end{aligned} \tag{170}$$

$$\begin{aligned} \operatorname{Im}\Lambda^{11}_{t}(\lambda_0,\lambda_0^*) = -\operatorname{Im}\Bigg(\Bigg(&Q_\parallel^2 + |Q^{11}_\perp|^2 - \\ &- \frac{(\mathbf{Q}_\parallel \mathbf{q}_\parallel + Q^{11}_\perp \lambda_0)(\mathbf{Q}_\parallel \mathbf{q}_\parallel + Q^{11\,*}_\perp \lambda_0)}{q_\parallel^2 + \lambda_0^2} \Bigg) \frac{U(\lambda_0, z)}{|z|^2} \Bigg), \end{aligned} \tag{171}$$

$$\Lambda^{1\,-1}_{l}(\lambda_0,-\lambda_0) = -\frac{\big((\mathbf{Q}_\parallel \mathbf{q}_\parallel)^2 - (Q^{11}_\perp \lambda_0)^2\big)\, U(\lambda_0, z)}{|z|^2 (q_\parallel^2 + \lambda_0^2)}, \tag{172}$$

$$\begin{aligned} \Lambda^{1\,-1}_{t}(\lambda_0,-\lambda_0) = -\Bigg(&Q_\parallel^2 - (Q^{11}_\perp)^2 - \\ &- \frac{(\mathbf{Q}_\parallel \mathbf{q}_\parallel)^2 - (Q^{11}_\perp \lambda_0)^2}{q_\parallel^2 + \lambda_0^2} \Bigg) \frac{U(\lambda_0, z)}{|z|^2}, \end{aligned} \tag{173}$$

with

$$Q^{11}_\perp = i\text{æ} + \bar{k}', \quad \lambda_0 = i\text{æ} + \bar{k}'_1. \tag{174}$$

The functions $\Phi_{l,t}$, which enter (169), are evident from (138).

A.2.5 Interim conclusion

The general formula for the inelastic cross section (62) for the initial sub-barrier neutrons is now fully defined with $\Pi_{l,t} = \Pi^{(1)}_{l,t} + \Pi^{(2)}_{l,t}$ given by (147) and (148) for the final state below the barrier ($k'_\perp < k_0$) or by (168) and (169) for that above the barrier ($k'_\perp > k_0$).

A.3 Inelastic transition probability for $\mathbf{G} = 0$

In this part of Appendix we calculate the dimensionless factor (70), which determines the inelastic transition prob-

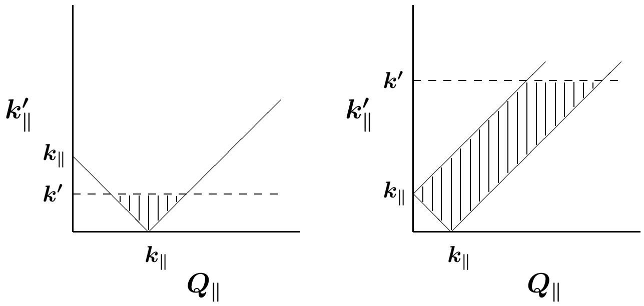

(a) **(b)**

Figure 7: Integration area for the double integral (175); the cases $k' < k_\parallel$ (a) and $k' > k_\parallel$ (b).

ability (69) with momentum transfer inside the first Brillouin zone ($\mathbf{G} = 0$).

In the integral (70) it is useful to replace the variable $k'_\perp$ by $k'^2_\parallel$ and the variable φ by $Q^2_\parallel = (\mathbf{k}'_\parallel - \mathbf{k}_\parallel)^2$ running from $(k'_\parallel - k_\parallel)^2$ up to $(k'_\parallel + k_\parallel)^2$. Thus,

$$W_{l,t}(k_\perp, k_\parallel \to \varepsilon') = \\ = \frac{k_\perp}{2\pi^2 k}\int dk'^2_\parallel \int dQ^2_\parallel\, g(Q_\parallel, k'_\parallel, k_\parallel)\, \frac{|t'|^2}{k'_\perp}\,\Pi_{l,t}, \qquad (175)$$

where the function g can be presented in two forms

$$g(Q_\parallel, k'_\parallel, k_\parallel) = \frac{1}{\sqrt{\left((k'_\parallel + k_\parallel)^2 - Q^2_\parallel\right)\left(Q^2_\parallel - (k'_\parallel - k_\parallel)^2\right)}} = \\ = \frac{1}{\sqrt{\left((Q_\parallel + k_\parallel)^2 - k'^2_\parallel\right)\left(k'^2_\parallel - (Q_\parallel - k_\parallel)^2\right)}}\,. \qquad (176)$$

Note, that

$$|t'|^2 = \begin{cases} 4k'^2_\perp/k^2_0, & k'_\perp < k_0, \\ 4k'^2_\perp/(k'_\perp + \bar{k}')^2, & k'_\perp > k_0. \end{cases} \qquad (177)$$

Integration area for double integral (175) is shown in Fig. 7.

The general formulae for the factors $\Pi_{l,t}$ are given by (147), (148) for the final state below the barrier ($k'_\perp < k_0$), and by (168), (169) for the final state above the barrier ($k'_\perp > k_0$). When $\mathbf{G} = 0$, the Eqs.(168) and (169) are simplified, and the sums of forward and backward scattering contributions can be written in the form

$$\Pi^{(1)}_l = \frac{1}{1 - r'^2}\left(-\frac{(Q^2_\parallel + |\lambda_0|^2)\,\mathrm{Im}\,U(\lambda_0, z)}{\text{æ}|z|^2} + \right. \\ \left. + \frac{r'}{|z|^2}\,\mathrm{Re}\,\frac{(Q^2_\parallel - \lambda^2_0)\,U(\lambda_0, z)}{\lambda_0}\right), \quad \Pi^{(1)}_t = 0. \qquad (178)$$

$$\Pi^{(2)}_{l,t} = \pm\frac{Q_\parallel\,\mathrm{Im}\,U(iQ_\parallel, z)}{(1 + r')|z|^2}, \qquad (179)$$

where $\lambda_0 = i\text{æ} + \bar{k}'$.

A.3.1 Estimations for variables and functions

The function $U(\alpha, z)$ (126) in (178) and (179) represents the correlation function. The real and imagine parts of the variable $z = x + iy$ are determined by the equations

$$2xy = \Gamma^2, \quad y^2 - x^2 = Q^2_\parallel - \frac{\epsilon\,\omega^2}{c^2}. \qquad (180)$$

With the fixed initial and final neutron energies, ε and ε', the "damping factor" Γ^2 (see Section 3) may be treated as the constant (defined by appropriate physics). The same is true for the quantity $\epsilon\,\omega^2/c^2$. It is convenient to use one of these parameters as a unit and transform all variables to the dimensionless form ($k'_\parallel \to \tilde{k}'_\parallel$, $Q_\parallel \to \tilde{Q}_\parallel$, $\Pi_{l,t} \to \tilde{\Pi}_{l,t}$ etc.). We choose as the unit $\Gamma/\sqrt{2}$, thus, e.g.,

$$x \to \tilde{x} = \frac{\sqrt{2}x}{\Gamma}, \quad y \to \tilde{y} = \frac{\sqrt{2}y}{\Gamma}, \quad Q_\parallel \to \tilde{Q}_\parallel = \frac{\sqrt{2}Q_\parallel}{\Gamma}, \qquad (181)$$

and, in particular,

$$\tilde{\omega}^2 \equiv \frac{2\epsilon\,\omega^2}{\Gamma^2 c^2}. \qquad (182)$$

Note, that $\epsilon = 1$, except for the longitudinal thermo-diffusion mode (see text after (41)), where $\epsilon = 0$. In the integral (175) the upper limit for $\tilde{k}'^2_\parallel$ is

$$\tilde{k}'^2 = \frac{2k'^2}{\Gamma^2}. \qquad (183)$$

The equations (180) take the form

$$\tilde{x}\tilde{y} = 1, \quad \tilde{y}^2 - \tilde{x}^2 = \tilde{Q}^2_\parallel - \tilde{\omega}^2. \qquad (184)$$

They define the functions $\tilde{x}(\tilde{Q}_\parallel)$ and $\tilde{y}(\tilde{Q}_\parallel)$ provided the parameter $\tilde{\omega}^2$ is given. Therefore, for our problem (with fixed ε and ε'), there is only one additional parameter, $\tilde{\omega}^2$, which should be specified by the physics of the process.

The damping factors Γ^2 for longitudinal sound waves both for solids and liquids (24) and for transverse sound waves for solids (25), as a rule, are much less than k'^2. On the other hand, in the diffusion-like cases (34) and (37) the damping factor takes the form

$$\Gamma^2 = \frac{|\omega|}{D} = \frac{2m|\varepsilon' - \varepsilon|}{\hbar^2 d}, \quad d = \frac{2mD}{\hbar}, \qquad (185)$$

where $D = D_S$ for longitudinal thermo-diffusion both for solids and liquids, and $D = \nu$ for damping transverse waves in liquids. Parameter d is dimensionless. It means, that (183) can be presented as

$$\tilde{k}'^2 = \frac{2\varepsilon' d}{|\varepsilon' - \varepsilon|}. \qquad (186)$$

Note, that in all realistic cases $d \gg 1$ (see Section 7). Therefore, both for sound-like and diffusion-like modes one has

$$\tilde{k}'^2 \gg 1. \tag{187}$$

The following relationship

$$\tilde{\omega}^2 \ll \tilde{k}'^2, \tag{188}$$

is also of great importance. Indeed,

$$\frac{\omega^2}{c^2} \approx \frac{\varepsilon'^2}{\hbar^2 c^2} = \frac{\varepsilon'}{2mc^2}\, k'^2 \ll k'^2, \tag{189}$$

because ε' is restricted from above by the Debye energy

$$\varepsilon_D = \hbar c (6\pi^2 n)^{1/3}, \tag{190}$$

and $\varepsilon_D \ll 2mc^2$ for all substances.

Let us separate two regions of integration oveq $\tilde{Q}_\parallel$ in (175): (I), where $\tilde{Q}_\parallel \sim \tilde{k}' \gg 1$ and $\tilde{\omega}$ (see (187) and (188)), therefore,

$$\text{(I)} \quad \tilde{x} \ll 1 \ll \tilde{y} \sim \tilde{Q}_\parallel \sim \tilde{k}', \tag{191}$$

and (II), where $\tilde{Q}_\parallel \ll \tilde{k}'$, therefore (see (187) and (188)),

$$\text{(II)} \quad \tilde{x}, \tilde{y}, \tilde{Q}_\parallel \ll \tilde{k}'. \tag{192}$$

In the region (I) the factor $\Pi^{(2)}_{l,t}$ (148) and (179) is of the scale

$$\tilde{\Pi}^{(2)}_{l,t} \sim \frac{1}{\tilde{y}^3} \sim \frac{1}{\tilde{Q}^3_\parallel} \ll 1. \tag{193}$$

The explicit form of the factor $\tilde{\Pi}^{(1)}_l$ in the same region depends on whether small or large energy transfers. For small the energy transfer, $\tilde{y} \sim \tilde{Q}_\parallel \sim \tilde{k}' \sim \tilde{\ae}$, and one has

$$\tilde{\Pi}^{(1)}_l \sim \frac{1}{\tilde{Q}^3_\parallel} \ll 1 \tag{194}$$

both from (147) and (178). The case of the large energy transfer corresponds to the relations: $\tilde{\ae} \sim \tilde{k}_0 \ll \tilde{y} \sim \tilde{Q}_\parallel \sim \tilde{k}'$. In this case only the region $k'_\perp > k_0$ is of interest. Therefore, one obtains from (178)

$$\tilde{\Pi}^{(1)}_l \simeq \frac{4\left(\tilde{Q}^2_\parallel + \tilde{k}'^2_\perp\right)}{\tilde{\ae}\left(\tilde{k}'^2_\perp + \tilde{y}^2\right)^2}. \tag{195}$$

Note, that this term dominates due to the relatively small factor $\tilde{\ae}$ in its denominator.

Now let us consider the region (II). The dimensionless factor $\tilde{\Pi}^{(2)}_{l,t}$ both below and above the barrier may be written in the form

$$\tilde{\Pi}^{(2)}_{l,t} = \mp \frac{\phi' \tilde{x} \tilde{Q}_\parallel (\tilde{Q}_\parallel + 2\tilde{y})}{|\tilde{z}|^2 \left(\tilde{x}^2 + (\tilde{Q}_\parallel + \tilde{y})^2\right)}, \tag{196}$$

where

$$\phi' = \begin{cases} 1, & k'_\perp < k_0, \\ (k'_\perp + \bar{k}')/k'_\perp, & k'_\perp > k_0. \end{cases} \tag{197}$$

The factor (147), (178) for the small energy transfer takes the form

$$\tilde{\Pi}^{(1)}_l \simeq \frac{\phi' \tilde{x}}{|\tilde{z}|^2}. \tag{198}$$

But it cannot be substantially simplified for large energy transfer. However, this is of no importance. Indeed, in this case the main contribution to the cross section comes from the region (I) due to the dominating term (195).

A.3.2 Estimation of the integral

Let us now estimate the integral (175). We see that the region (I) contributes only to the factor W_l for the large energy transfer due to (195). Since $k' \sim Q_\parallel \gg \ae \sim k_\parallel$, one can perform the integration over $k'_\parallel$ in (175) in the narrow interval $Q_\parallel - k_\parallel < k'_\parallel < Q_\parallel + k_\parallel$ (see Fig. 7b). It gives

$$W^{(I)}_l(k_\perp, k_\parallel \to \varepsilon') \simeq \frac{k_\perp}{2\pi k} \int d\tilde{Q}^2_\parallel \, \frac{|t'|^2}{\tilde{k}'_\perp}\, \tilde{\Pi}^{(1)}_l, \tag{199}$$

where $\tilde{k}'_\perp = \sqrt{\tilde{k}'^2 - \tilde{Q}^2_\parallel}$, and $\tilde{\Pi}^{(1)}_l$ is given by (195). Taking into account (184) and (191) and integrating over $\tilde{Q}^2_\parallel$ from $\tilde{\omega}^2$ to $\tilde{k}'^2$, one obtains

$$W^{(I)}_l(k_\perp, k_\parallel \to \varepsilon') \simeq \frac{2k_\perp \Gamma^2 k'^2}{\pi k \ae \left(k'^2 - \epsilon\, \omega^2/c^2_l\right)^{3/2}}\,, \tag{200}$$

where the result is presented in terms of the physical quantities.

Now let us consider the contribution to the cross section from the region (II). It is convenient to rewrite the factor (175) as follows

$$W_{l,t}(k_\perp, k_\parallel \to \varepsilon') = \frac{k_\perp}{2\pi^2 k} \int d\tilde{Q}^2_\parallel \frac{\tilde{\Pi}_{l,t}}{\phi'} \int d\tilde{k}'^2_\parallel \, \tilde{g} \tilde{f}(k'_\perp), \tag{201}$$

where the function $\tilde{\Pi}_{l,t}/\phi'$ given by (196) and (198) depends only on $\tilde{Q}^2_\parallel$, and

$$f(k'_\perp) \equiv \frac{\phi' |t'|^2}{k'_\perp} = \frac{4}{k^2_0}\left(k'_\perp - \theta(k'^2_\perp - k^2_0)\sqrt{k'^2_\perp - k^2_0}\,\right), \tag{202}$$

with $\theta(x) = 0$ for $x < 0$ and $\theta(x) = 1$ for $x \geq 0$.

The integral over $\tilde{k}'^2_\parallel$ is of the form

$$\int d\tilde{k}'^2_\parallel \, \tilde{g} \tilde{f}(k'_\perp) = \frac{4}{\tilde{k}^2_0}\left(I(\tilde{k}') - I(\sqrt{\tilde{k}'^2 - \tilde{k}^2_0}\,)\right), \tag{203}$$

where

$$I(b) = \theta(b^2 - \tilde{k}^2_\parallel) \int d\tilde{k}'^2_\parallel \, \tilde{g}\; \theta(b^2 - \tilde{k}'^2_\parallel)\sqrt{b^2 - \tilde{k}'^2_\parallel}. \tag{204}$$

The variable $\tilde{k}'^2_\parallel$ runs from $(\tilde{Q}_\parallel - \tilde{k}_\parallel)^2$ up to $(\tilde{Q}_\parallel + \tilde{k}_\parallel)^2$ (see Fig. 7). Then, $I(b)$ can be presented in terms of elliptic integral

$$I(b) = 2\,\theta(b^2 - \tilde{k}_\parallel^2)\,\beta E(\frac{\alpha^2}{\beta^2}),\ \ E(m) = \int\limits_0^{\pi/2} \sqrt{1 - m\sin^2\theta}\, d\theta, \tag{205}$$

where

$$\alpha^2 = 4\tilde{Q}_\parallel \tilde{k}_\parallel, \quad \beta^2 = b^2 - (\tilde{Q}_\parallel - \tilde{k}_\parallel)^2. \tag{206}$$

It is of importance, that in the region (II) both for small and large energy transfer one has

$$\tilde{Q}_\parallel \tilde{k}_\parallel \ll \tilde{k}'\tilde{k}_\parallel \leq \tilde{k}'^2 - \tilde{k}_0^2,\, \tilde{k}'^2 \quad \Longrightarrow \quad \alpha \ll \beta. \tag{207}$$

Then, really $E(\alpha^2/\beta^2) \simeq \pi/2$, and, therefore, the contribution from the region (II) to the cross section is

$$W_{l,t}^{(II)}(k_\perp, k_\parallel \to \varepsilon') \simeq \frac{k_\perp}{2\pi k} \int d\tilde{Q}_\parallel^2 \, \frac{|t'|^2}{\tilde{k}'_\perp}\, \tilde{\Pi}_{l,t}, \tag{208}$$

where $\tilde{k}'_\perp = \sqrt{\tilde{k}'^2 - (\tilde{Q}_\parallel - \tilde{k}_\parallel)^2} \simeq \sqrt{\tilde{k}'^2 - \tilde{k}_\parallel^2}$, while $\tilde{\Pi}_l^{(1)}$ and $\tilde{\Pi}_{l,t}^{(2)}$ are given by (198) and (196), respectively.

To calculate the integral it is convenient to replace $\tilde{Q}_\parallel^2$ by $\tilde{x}$ with the use of

$$d\tilde{Q}_\parallel^2 = -\frac{2|\tilde{z}|^2}{\tilde{x}}\, d\tilde{x}. \tag{209}$$

The limit $\tilde{Q}_\parallel = 0$ corresponds to

$$\tilde{x}_0^2 = \sqrt{\frac{\tilde{\omega}^4}{4} + 1} + \frac{\tilde{\omega}^2}{2}. \tag{210}$$

In the opposite limit $\tilde{Q}_\parallel \to \infty$, $\tilde{x} \to 0$, then the integral (208) can be presented in the form

$$W_l^{(II)}(k_\perp, k_\parallel \to \varepsilon') = \frac{k_\perp}{\pi k}\, \tilde{f}(k'_\perp) \left(\tilde{J}^{(1)} - \tilde{J}^{(2)}\right), \tag{211}$$

$$W_t^{(II)}(k_\perp, k_\parallel \to \varepsilon') = \frac{k_\perp}{\pi k}\, \tilde{f}(k'_\perp)\, \tilde{J}^{(2)}, \tag{212}$$

where

$$\tilde{J}^{(1)} = \tilde{x}_0, \quad \tilde{J}^{(2)} = \int\limits_0^{\tilde{x}_0} \frac{\tilde{Q}_\parallel(\tilde{Q}_\parallel + 2\tilde{y})}{\tilde{x}^2 + (\tilde{Q}_\parallel + \tilde{y})^2}\, d\tilde{x}. \tag{213}$$

Straightforward calculation gives

$$\tilde{J}^{(2)} = \frac{2\tilde{x}_0}{3}. \tag{214}$$

Then, summing the contributions from the regions (I) and (II) we get in terms of the physical quantities the results (74)–(78).

A.4 Inelastic transition probability for $\mathbf{G} \neq 0$

In this part of Appendix we calculate the dimensionless factor (73), which determines the inelastic transition probability (72) with the momentum transfer $\mathbf{G}$ to the crystal lattice. The final neutron energy $\varepsilon' \simeq \hbar^2 G^2/2m$ is much larger than the barrier energy U and initial energy ε, thus

$$\mathbf{k}'_\parallel \simeq -\mathbf{G}_\parallel, \quad \bar{k}' \simeq k'_\perp \simeq G_\perp \gg æ, \quad r' \to 0, \quad t' \to 1. \tag{215}$$

The Π factors (168) and (169) have now equal contributions from backward and forward scattering and, with the help of approximations (215) and expression (170)–(174), (138), take the form

$$\Pi_l^{(1)} = -\frac{1}{æ|z|^2}\, \mathrm{Im}\left(\frac{\left(\mathbf{G}_\parallel \mathbf{q}_\parallel + G_\perp \lambda_0\right)^2 U(\lambda_0, z)}{q_\parallel^2 + \lambda_0^2}\right), \tag{216}$$

$$\begin{aligned} \Pi_t^{(1)} = &-\frac{G^2\, \mathrm{Im}\, U(\lambda_0, z)}{æ|z|^2} + \\ &+ \frac{1}{æ|z|^2}\, \mathrm{Im}\left(\frac{\left(\mathbf{G}_\parallel \mathbf{q}_\parallel + G_\perp \lambda_0\right)^2 U(\lambda_0, z)}{q_\parallel^2 + \lambda_0^2}\right), \end{aligned} \tag{217}$$

$$\begin{aligned} \Pi_{l,t}^{(2)} = \pm &\frac{q_\parallel^2 |\mathbf{G}_\parallel \mathbf{q}_\parallel + G_\perp \lambda_0|^2 - |\lambda_0 \mathbf{G}_\parallel \mathbf{q}_\parallel - G_\perp q_\parallel^2|^2}{|q_\parallel^2 + \lambda_0^2|^2} \times \\ &\times \frac{\mathrm{Im}\, U(iq_\parallel, z)}{q_\parallel |z|^2}, \end{aligned} \tag{218}$$

where

$$\lambda_0 = iæ + \xi_\perp, \quad \xi_\perp = k'_\perp - G_\perp. \tag{219}$$

The integral (73) is over the Brillouin zone with the center in $\mathbf{G}$. It is convenient to take

$$d^3k' = dk'_\perp d^2k'_\parallel \to d\xi_\perp d^2 q_\parallel, \tag{220}$$

because $\mathbf{q}_\parallel = -\mathbf{k}'_\parallel - \mathbf{G}_\parallel$. Integration over the angle between $\mathbf{q}_\parallel$ and $\mathbf{G}_\parallel$ gives

$$\langle \mathbf{G}_\parallel \mathbf{q}_\parallel \rangle = 0, \quad \langle \left(\mathbf{G}_\parallel \mathbf{q}_\parallel\right)^2 \rangle = \frac{G_\parallel^2 q_\parallel^2}{2}\,. \tag{221}$$

Then the W factors take the form

$$\begin{aligned} W_{l,t}^{(1)}(k_\perp, k_\parallel \to \mathbf{G}) = &\frac{k_\perp}{\pi k æ G^2} \int d\xi_\perp dq_\parallel^2 \times \\ \times \Bigg(\mp &\frac{q_\parallel^2 \left(G_\parallel^2/2 - G_\perp^2\right)}{|z|^2}\, \mathrm{Im}\left(\frac{U(\lambda_0, z)}{q_\parallel^2 + \lambda_0^2}\right) - \\ &- \frac{G_{\perp,\parallel}^2\, \mathrm{Im}\, U(\lambda_0, z)}{|z|^2}\Bigg), \end{aligned} \tag{222}$$

$$\begin{aligned} W^{(2)}_{l,t}(k_\perp, k_\parallel \to \mathbf{G}) = \pm \frac{k_\perp}{\pi k G^2} \int d\xi_\perp dq^2_\parallel \times \\ \times \frac{q_\parallel \left(G^2_\parallel/2 - G^2_\perp\right)(q^2_\parallel - |\lambda_0|^2)\,\mathrm{Im}\,U(iq_\parallel, z)}{|z|^2 |q^2_\parallel + \lambda^2_0|^2}. \end{aligned} \tag{223}$$

Now we can integrate over $\xi_\perp$ transforming the integrals into contour ones by closing a path in the complex $\xi_\perp$ plane. For three functions to be integrated, one easily obtains

$$\int d\xi_\perp\, \mathrm{Im}\left(\frac{U(\lambda_0, z)}{q^2_\parallel + \lambda^2_0}\right) = \begin{cases} 0, & q_\parallel < \ae, \\ \pi\, \mathrm{Im}\,U(iq_\parallel, z)/q_\parallel, & q_\parallel > \ae, \end{cases} \tag{224}$$

$$\int d\xi_\perp\, \mathrm{Im}\,U(\lambda_0, z) = -2\pi x, \tag{225}$$

$$\int d\xi_\perp \frac{q^2_\parallel - |\lambda_0|^2}{|q^2_\parallel + \lambda^2_0|^2} = \begin{cases} -\pi/\ae, & q_\parallel < \ae, \\ 0, & q_\parallel > \ae. \end{cases} \tag{226}$$

Using these results we get for the sum of $W^{(1)}$ and $W^{(2)}$ factors

$$\begin{aligned} W_{l,t}(k_\perp, k_\parallel \to \mathbf{G}) = \mp \frac{k_\perp \left(G^2_\parallel/2 - G^2_\perp\right)}{k\ae G^2} \times \\ \times \int dq^2_\parallel \frac{q_\parallel\, \mathrm{Im}\,U(iq_\parallel, z)}{|z|^2} + \\ + \frac{2k_\perp G^2_{\perp,\parallel}}{k\ae G^2} \int dq^2_\parallel \frac{x}{|z|^2}. \end{aligned} \tag{227}$$

Using (131) and (209), one obtains

$$\int dq^2_\parallel \frac{q_\parallel\, \mathrm{Im}\,U(iq_\parallel, z)}{|z|^2} = -4J^{(2)}, \tag{228}$$

$$\int dq^2_\parallel \frac{x}{|z|^2} = 2J^{(1)}, \tag{229}$$

where $J^{(1)}$ and $J^{(2)}$ are given by (214). Thus, the W factors are of the form (79) and (80).

References

[1] V. I. Luschikov, Y. N. Pokotilovsky, A. V. Strelkov, F. L. Shapiro, Sov. Phys. JETP Lett. **9**, 23 (1969).

[2] A. Steyerl, Phys. Lett. B, **29**, 33 (1969).

[3] R. Golub, Rev. Mod. Phys. **68** 329 (1996).

[4] E. Korobkina, R. Golub, J. Butterworth, P. Geltenbort, S. Arzumanov, Phys. Rev. B **70** 035409 (2004).

[5] A. V. Strelkov, V. V. Nesvizhevsky, P. Geltenbort, D. G. Kartashov, A. G. Kharitonov, E. V. Lychagin, A. Yu. Muzychka, J. M. Pendlebury, K. Schreckenbach, V. N. Shvetsov, A. P. Serebrov, R. R. Taldaev, P. Yaidjiev, Nucl. Instr. Meth. A **440**, 695 (2000).

[6] L. N. Bondarenko, P. Geltenbort, E. I. Korobkina, V. I. Morozov, Yu. N. Panin, Phys. At. Nucl. **65**, 11 (2002).

[7] E. V. Lychagin, D. G. Kartashov, A. Yu. Muzychka, V. V. Nesvizhevsky, G. V. Nekhaev, A. V. Strelkov, Phys. At. Nucl. **65**, 1995 (2002).

[8] A. Steyerl, B. G. Yerozolimsky, A. P. Serebrov, P. Geltenbort, N. Achiwa, Yu. N. Pokotilovski, O. Kwon, M. S. Lasakov, I. A. Krasnoshchokova, A. V. Vasilyev, Eur. Phys. J. B **28**, 299 (2002).

[9] A. P. Serebrov, J. Butterworth, M. Daum, A. K. Fomin, P. Geltenbort, K. Kirch, I. A. Krasnoschekova, M. S. Lasakov, Yu. P. Rudnev, V. E. Varlamov, A. V. Vassiljev, Phys. Lett. A **309**, 218 (2003).

[10] S. K. Lamoreaux, R. Golub, Phys. Rev. C **66**, 044309 (2002).

[11] L. Van Hove, Phys. Rev. **95**, 249 (1954).

[12] I. I. Gurevich, L. V. Tarasov, *Low-Energy Neutron Physics* (Amsterdam, North Holland Pub. Co., 1968).

[13] S. W. Lovesey, *Theory of Neutron Scattering from Condensed Matter*, vols. 1 and 2 (Oxford, Clarendon Press 1984)

[14] A. L. Barabanov, S. T. Belyaev, Eur. Phys. J. B **15**, 59 (2000).

[15] V. K. Ignatovich, *The Physics of Ultracold Neutrons* (Oxford, Clarendon Press, 1990).

[16] R. Golub, D. Richardson, S. K. Lamoreaux, *Ultracold Neutrons* (Adam Hilger, Bristol, Philadelphia and New York, IOP Publishing Ltd, 1991).

[17] D. I. Blokhintzev, N. M. Plakida, Phys. Status Solidi B **82**, 627 (1977); Preprint JINR P4-9631 (Dubna, JINR, 1976) (in Russian); Preprint JINR P4-10381 (Dubna, JINR, 1977) (in Russian).

[18] V. K. Ignatovich, M. Utsuro, Nucl. Instr. Methods A **440**, 709 (2000).

[19] A. Serebrov, N. Romanenko, O. Zherebtsov, M. Lasakov, A. Vasiliev, A. Fomin, P. Geltenbort, I. Krasnoshekova, A. Kharitonov, V. Varlamov, Phys. Lett. A **335**, 327 (2005).

[20] A. L. Barabanov, K. V. Protasov, nucl-th/0507020, Phys. Lett. A, in press.

[21] Yu. N. Pokotilovski, Eur. Phys. J. B **8**, 1 (1999).

[22] Yu. N. Pokotilovski, Phys. Lett. A **255**, 173 (1999).

[23] P. Schofield, In: *Physics of Simple Liquids*, Eds. H. N. V. Temperley, J. S. Rowlinson, G. S. Rushbrooke (North-Holland Publishing Company, Amsterdam, 1968).

[24] D. Forster, *Hydrodynamic Fluctuations, Broken Symmetry, and Correlation Functions* (W.A.Benjamin, Inc., Advanced Book Program Reading, Massachusetts, London, Amsterdam, Don Mills, Ontario, Sidney, Tokyo, 1975).

[25] A. I. Akhiezer, S. V. Peletminskii, *Methods of statistical physics* (Pergamon Press, Oxford, New York, 1981).

[26] L. D. Landau, E. M. Lifshitz, A. P. Pitaevskii, *Statistical physics* v.2 (Pergamon Press, Oxford, New York, 1986).

[27] L. D. Landau, E. M. Lifshitz, A. M. Kosevich, L. P. Pitaevskii, *Theory of elasticity* (Pergamon Press, Oxford, New York, 1986).

[28] B. Ya. Balagurov, V. G. Vaks, ZETPh **57**, 1646 (1969).

[29] Ia.I.Frenkel', *Kinetic theory of liquids* (Oxford, Clarendon Press, 1946).

[30] V. V. Nesvizhevsky, Phys. At. Nucl. **65**, 400 (2002).